

Reply to referee Thomas Rahn comments

Ref. Com. Line 25: *The 1940 atmospheric mole fraction, and hence the growth rate, differs from the determined by Battle et al. (1996) and to a lesser degree with Machida et al. 1995 please discuss (discussion section).*

Author's Resp.: Following the referee's suggestion we have added a discussion (see below) in the discussion section.

"The N₂O mole fraction atmospheric history from our multi-site reconstruction is in agreement with recent work from Meinshausen et al. (2016) who combined all available published N₂O data (atmospheric, firn, ice) in order to reconstruct a historical atmospheric record of the past 2000 years. It differs slightly from the one determined by Battle et al. (1996) and to smaller extent with Machida et al. (1995).

Battle et al. (1996) collected firn air data and Machida et al. (1995) used ice data. Both studies used samples from a single Antarctic site. One could argue that the difference is due to an interhemispheric difference, but it is too large to be explained by this alone. In the past, N₂O mole fraction measurements have been reported on different calibration scales, which is likely to explain part of the differences between individual studies. Furthermore, differences in the firn air model and possible differences between sites may contribute. In our case we used measurements from 5 sites to constrain our model while Battle et al. (1996) and Machida et al. (1995) used only one site. In addition, the atmospheric histories of up to 9 known gases (depending on site, Witrant et al. 2012) were used to constrain diffusivity in our model while Battle et al. (1996) only used two gases."

Author's changes: Lines 549-563, Lines 738-740, Lines 811-813

Ref. Com. Line 48: *N₂O as a source of stratospheric NO_x was certainly known prior to Ravishankara's 2009 work see McElroy, Khalil, Crutzen, etc.*

Author's Resp.: The following references have been added to the manuscript: McElroy, M. B., and McConnell, J. C.: Nitrous Oxide: A natural source of stratospheric NO, *Journal of Atmospheric Sciences*, 28, 1095-1098, 1971.

Crutzen, P. J.: The role of NO and NO₂ in the chemistry of the troposphere and stratosphere, *Annual review of earth and planetary sciences*, 7, 443-472, 1979.

Author's changes: Line 46, Lines 760-761, Lines 822-823

Ref. Com. Lines 80-81: *Rahn and Wahlen (1997) also contributed here with the first reference that describes a fractionation factor for stratospheric loss.*

Author's Resp.: The suggested reference has been added to the revised manuscript. Rahn, T., and Wahlen, M.: Stable isotope enrichment in stratospheric nitrous oxide, *Science*, 278, 1776-1778, doi: 10.1126/science.278.5344.1776, 1997.

Author's changes: Line 79, Lines 865-866

Ref. Com. Lines 82-84: *Rahn et al. (1998) also contributed here with the first laboratory verification of wavelength dependent kinetic fractionation during photolysis.*

Author's Resp.: The suggested reference has been added to the revised manuscript. Rahn, T., Zhang, H., Wahlen, M., and Blake, G. A.: Stable isotope fractionation during ultraviolet photolysis of N₂O, *Geophys. Res. Lett.*, 25, 4489-4492, 1998.
Author's changes: Line 83, Lines 867-868

Ref. Com. Line 116: "Carbon composition of"?

Author's Resp.: We corrected this omission and replaced it with "of its carbon composition".

Author's changes: Line 115

Ref. Com. Lines 141-142: For my own edification, doesn't this require dual bladders so that a specific depth range can be isolated?

Author's Resp.: When firn samples are collected with this method, a new hole is drilled from the top. The hole is drilled to a certain depth and then the bladder is inserted down close to the bottom of the drill hole, so in practice the bottom of the drill hole plays the role of the second bladder that the referee indicated.

Ref. Com. Lines 270-275: Mole fraction data from NEEM is substituted for, with CSIRO/IUP/CIC/NOAA data. Does this induce a simple offset or a trending offset? In either case by how much?

Author's Resp.: NEEM data measured at IMAU was replaced by IUP/CIC/NOAA and CSIRO because IMAU data is less precise. The atmospheric trend reconstruction from IMAU-NEEM data, shown in black, in Fig. 1 has larger uncertainties than the trend scenario based on the more precise IUP/CIC/NOAA/CSIRO data (in red). The IMAU data based scenario is smoother because the model can reconstruct less details from more uncertain data. Thus the replacement of IMAU data with IUP/CIC/NOAA/CSIRO data does not induce an offset but leads to a more accurate and less smoothed output scenario.

Author's changes: Lines 274-276, Lines 468-469, Lines 1018-1019, Lines 1029-1030, Lines 1160-1161, Lines 1183-1184

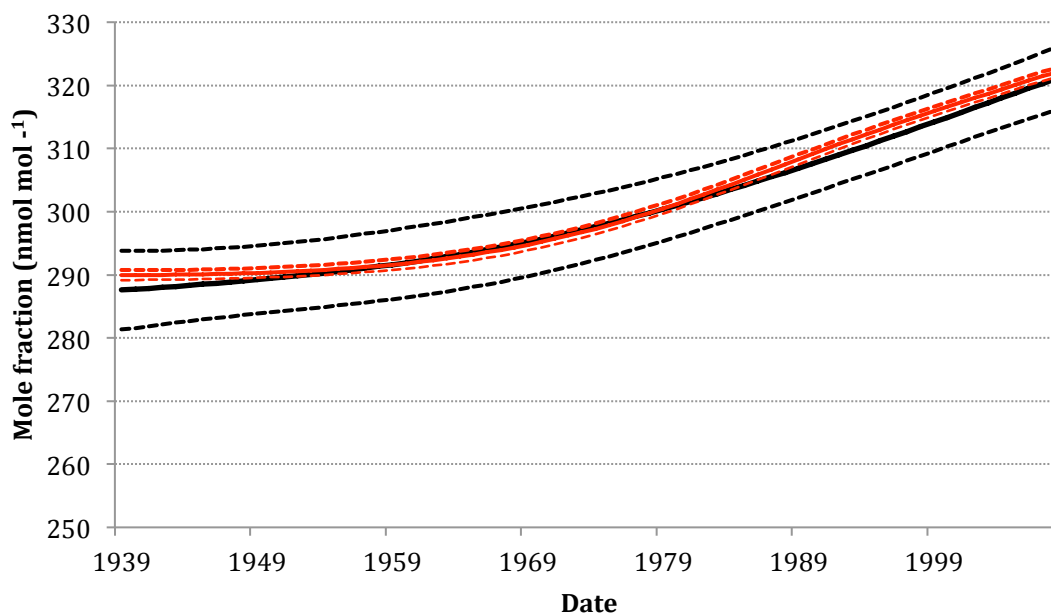


Figure 1: Firm air trend reconstruction using only NEEM measurements from IMAU laboratory (black line) with uncertainty envelopes (dashed black lines) compared to firm air trend reconstruction using NEEM measurements from IUP/CIC/NOAA and CSIRO atmospheric (red line) with corresponding uncertainty envelopes (dashed red lines).

Ref. Com. Lines 289-299: *The natural sources from land and sea have quite different production mechanisms as well as previously observed and predicted different isotopic signatures (Kim and Craig, 1993; Rahn and Wahlen, 2000; and others) yet the isotopic model used here lumps all natural source into a single term. Given the detailed history that the authors are attempting to tease apart, this seems to me detrimental to their efforts. Please justify keeping the natural source as a single term. This should also be elaborated on further in the discussion section.*

Author's Resp.: Yes, the isotope signatures of natural and terrestrial sources are different, and this has indeed been used to reconstruct contributions of marine and terrestrial sources to N₂O variations in the past (Schilt et al., 2014). In the present study we focus on the change since pre-industrial times, where the strong increase in the N₂O mole fraction suggests that this increase is dominated anthropogenic activities. Therefore we apply a model that assumes that the natural source strength has remained constant. This is clearly stated in the paper, but we have added some additional comments in the revised version. We would of course like to be able to differentiate between more processes, but our result indicates that with the present analytical precision, and given the uncertainties in source signatures, it is not really adequate to constrain additional degrees of freedom. In response to the referee comment we have added in the discussion that changes in natural sources that occur in parallel to the anthropogenic emissions cannot be distinguished with our approach, but may as well influence the results.

Author's changes: Lines 333-338, Lines 598-599

Ref. Com. Line 326: *As well as Rahn and Wahlen 2000*

Author's Resp.: The suggested reference has been added to the revised manuscript. Rahn, T., and Wahlen, M.: A reassessment of the global isotopic budget of atmospheric nitrous oxide, *Glob. Biogeochem. Cycl.*, 14, 537-543, 2000.

Author's changes: Line 326, Lines 869-870

Ref. Com. Lines 429-439: *Discussion of interlaboratory variability. The authors state that discrepancies do not exhibit a systematic shift and that Sowers et al. data had good agreement between two different laboratories but then they leave this conundrum hanging. Please elaborate a little on possibilities.*

Author's Resp.: We realize that this is not fully satisfactory, but we have investigated this in quite some detail and cannot resolve the discrepancies. A possible origin of the difference could be based on the reconstruction model. Because the uncertainties on the South Pole data are large, compared to the other sites, the multi-site homogenization is more uncertain and less efficient (see Appendix A and C, Fig. A1 and C1-C3). Sampling uncertainty should also be taken into consideration since when pumping firn air and filling the sampling flasks you could encounter uncertainties (contamination, possible leak, fractionation, incomplete flask flushing etc). We have added this as additional discussion to the text.

Author's changes: Lines 438-444

Ref. Com. Line 457: *Regularization term is increased by how much?*

Author's Resp.: The regularization factor was increased by a factor of 10. This was added in the revised manuscript.

Author's changes: Lines 461-463, Line 635, Line 1098

Ref. Com. Lines 469-470: *I find this paragraph confusing. The average annual emission of 3.5 TgN/yr in the last sentence should be the difference between 1940-2008 should it not? But there the difference is 4.4 TgN/yr. I think I am confused because in the one case the natural term is included but in the other they are only considering the anthropogenic. In any case, this entire paragraph could be presented with more clarity.*

Author's Resp.: We have reworded this paragraph to remove the confusion. The average annual emission of 3.5 TgN/yr corresponds to the annual growth rate of 0.7 nmol mol⁻¹ a⁻¹ calculated between years 1995 and 2008. The total change the N₂O mole fraction of (32±1) nmol mol⁻¹ can be explained in the mass balance model by a (4.4±1.7) Tg a⁻¹ N increase in the emissions from in 1940 to 2008. The paragraph has been updated to state the above clearly.

Author's changes: Lines 474-476

Ref. Com. Lines 488-495 and lines 587-595: *Observation of decadal variability in $\delta^{15}\text{N}_{\text{av}}$ and discussion of changes in relative contribution of sources over time. If real, this is possibly the most important observation in the manuscript and needs to be dealt with much more considered manner. Intuitively, one would agree with their statement i.e. that the agricultural source would imprint the record more significantly in the earlier part of the record and decrease, in a relative sense, over time. This would mean that yes, the earliest human influences would be significantly depleted.*

As time goes on, fertilizer use becomes more controlled leading to less overuse and more limited flux of N₂O accompanied by less isotopic discrimination. This along with increased industrial production of N₂O would hypothetically lead the observed increase in $\delta^{15}\text{N}_{\text{anh}}$ over time (both avg and beta). This increase (Fig. 4, right) peaks in the late 1980's however and proceeds to decrease significantly (~10% for $\delta^{15}\text{N}_{\text{av}}$ and ~20% for $\delta^{15}\text{N}_{\text{b}}$). This decrease is much more difficult to explain in a qualitative sense and in truth is difficult to believe.

One possibility is that industries are doing a better job of decreasing and/or capturing fugitive emissions which might increase in the proportion of $\delta^{15}\text{N}$ depleted agriculture relative to industry but:

A. Is there evidence of this?

B. Would it yield this large of a result?

A more detailed discussion of this is warranted given the subtly profound implications including discussion of potential artifacts in measuring and modeling that could also lead the observed modeled record.

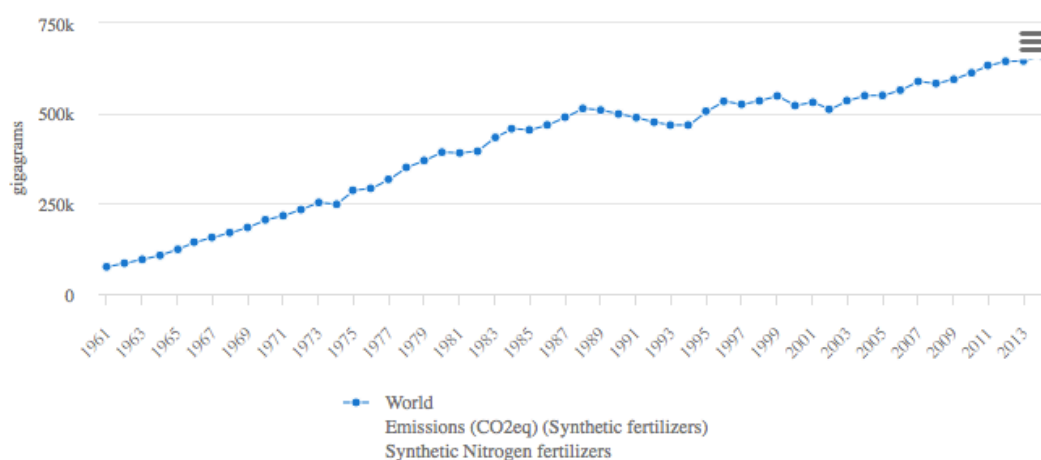
Author's Resp.: We thank the referee for this a comment. We actually tried to keep a balance between discussing possible scenarios (first part of the referee comment) and examine whether the reconstructed changes are realistic (second part of the referee comment). Independent quantitative evidence for some of the suggested changes is actually available from inventory information, which was not included in the original version of our manuscript. According to FAO statistics (<http://www.fao.org/faostat/en/#data/GY/visualize>), emissions from synthetic nitrogenous fertilizers increased between 1961 and 1985, then stayed relatively constant or even decreased until 2000, and increased again after 2000. The reasons of the decrease between 1985 and 2000 are a small turn to organic soil cultivation in combination with more efficient agricultural methods and fertilizer use. This qualitatively matches the temporal evolutions of our reconstructed source signatures, but as the referee points out the observed isotopic signature change after 1985 is quite large, especially for $\delta^{15}\text{N}_{\text{av}}$ and $\delta^{15}\text{N}_{\text{b}}$. This is why we did not discuss this in more detail in the original manuscript. In the revised version, we added this information, but also point out that this effect is likely not strong enough to explain the reconstructed isotope signal.

In the manuscript, we do discuss the fact that (part of) decadal variability may originate from small undulations on the reconstructed scenarios, since the emissions are related to the derivative of the trend. It is possible to draw straight lines within the uncertainty envelopes of the scenarios, and therefore the reconstructed decadal variability may not be robust but a product of the reconstruction procedure. Indeed, increasing the regularization term by a factor of 10 leads to much smoother (nearly straight) lines that fit inside the uncertainty envelopes. Therefore the decadal variability may not be realistic, and we do not want to put too much emphasis on the interpretation in terms of underlying processes. We realize that this is a bit unsatisfactory, but given the large uncertainties we think that the level of interpretation that we give is adequate. We do not want to put forward scenarios that are unrealistic and not really backed up by the data.

Author's changes: Lines 621-637

Emissions (CO₂ equivalent), Synthetic Nitrogen fertilizers

1961 - 2014



Ref. Com. Line 524: Starting value of $d18O_{anth}$, looks like about 8% to me but I am looking at Fig. 4 because there is no Fig. 5.

Author's Resp.: The mistake has been corrected and substituted with $(7.7 \pm 2.6) \%$.
Author's changes: [Line 529](#)

Ref. Com. Lines 552-562: The authors perform a sensitivity study of changing the lifetime but it seems to me that there should also be a sensitivity study on other terms, in particular F (exchange) which is a term that is poorly known. Also given the two box model that is being used it seems that more appropriate lifetime would be stratospheric lifetime in conjunction with X_{strat} given that this is the box where all N_2O destruction takes place.

Author's Resp.: Sensitivity tests on the magnitude of F_{exch} have been added in the Appendix D. The results show that when the F_{exch} value is low, then less N_2O is returned to the troposphere, contrary, when F_{exch} is high more N_2O is returned. The study showed that F_{exch} has little effect on the isotopic signature results, thus we concluded that only the flux is sensitive to the choice of F_{exch} value while the isotopic composition is not.

The use of global mean lifetime is correct because eq. 3 in the manuscript refers to the total atmospheric burden and not the stratospheric burden. The mean stratospheric lifetime would be about 10 times smaller than the global mean lifetime.

Author's changes: [Lines 582-586](#), [Lines 1117-1118](#), [Lines 1124-1126](#), [Lines 1140-1158](#), [Lines 1177-1205](#)

Ref. Com. Lines 563-573: This was also predicted by Rahn and Wahlen (2000), prior to any firn air measurements being made, where they predicted a -0.03 permil/yr trend in $15N_{av}$ (identical to that on the line 417) and a -0.03 permil/yr trend in $18O$ (-0.02 permil/yr on line 418 being within the estimated error).

Author's Resp.: This has been included in the revised manuscript.

Author's changes: Lines 595-596, Lines 869-870

Ref. Com. Lines 576-580: *The 'natural' component of the ocean source is estimated to be on the order of 4Tg N/yr. This new 'anthropogenic' component would then comprise a 25% increase in the ocean source. This gets back to my earlier comment on separating the natural source into land and ocean sources. Would this 'new' oceanic N₂O have an identical isotopic signature to the natural signature or would it be somehow different? In either case, it would certainly be distinct from the land signature. How would this be reflected in the temporal evolution of the firm records?*

Author Resp.: As mentioned above, we cannot really constrain more free parameters, and we have chosen to lump all parts of the “anthropogenic” source together. Here we discuss that variations in different components of the anthropogenic source may leave temporal signals in the source signature. Snider et al. (2015) made a meta-analysis of previously published source signature studies and concluded that freshwater bulk isotope signatures are (-7.78±9.72) ‰ and (40.75±9.63) ‰ for $\delta^{15}\text{N}^{\text{av}}$ and $\delta^{18}\text{O}$ respectively. Similarly for marine waters the results were (5.14±1.93) ‰ for $\delta^{15}\text{N}^{\text{av}}$ and (44.76±3.62) ‰ for $\delta^{18}\text{O}$. We feel that it is not possible at present to make a quantitative statement, given the available information both from bottom-up studies and isotope source signature studies, and therefore discuss these effects qualitatively only.

General comments:

Ref. Com.: *On two occasions reference is made to Fig. 5, but no Fig. 5 exists. I assume they refer to Fig. 4? In the Appendix: Fig. A1 caption, left and right are switched. Figures C1 and C2 appear to be switched, Fig. 3 (page 45) precedes Fig. C2 (page 47) and there is a Fig. 3 and a Fig. C3 (or is it Fig. C3 and C4?). This is all rather sloppy. It is difficult for the reader to tease apart which data sets are new analyses and which were previously published.*

Author's Resp.: We apologize for the mislabeling, and these errors were corrected in the revised version.

Author's changes: Line 485, Line 501, Line 517, Line 530, Line 589, Line 1044, Line 1046, Lines 1088-1092, Lines 1093-1096

Ref. Com.: *The new samples from NEEM are discussed thoroughly and the previously published data sets are referred to but nowhere is there an itemized tabulation of which data is associated with specific publications and which, other than NEEM, if any, are new.*

Author's Resp.: This information has been added in the revised manuscript in the revised Table 1.

Author's changes: Lines 953-960

Ref. Com.: *In addition, there are two different records from NGRIP-01, one which is included in the analysis and one which is not but both are referred to with the same sample name. Please add a subscript or some other differentiating factor so that the reader does not have to try and sort this out for himself.*

Author Resp.: The requested information has been added in the revised manuscript. A subscript indicating the differentiation between the two publications is used (NGRIP-01_{Ishijima}, NGRIP-01_{Bernard}) throughout the manuscript.

Author's changes: Line 211, Line 213, Line 393, Lines 428-429, Line 954, Line 999, Line 1013, Line 1015, Line 1044, Line 1045, Lines 1080-1087, Line 1091

Ref. Com.: Ultimately the authors conclude that 'Based on the changes in the isotopes we conclude that the main contribution to N₂O change in the atmosphere since 1940 is from soils, with agricultural soils being the principal anthropogenic component which is in line with previous studies'. Which is anticlimactic to say the least given the effort that went into sample collection, processing, analysis and modeling.

Author Resp.: We agree that this part of the conclusion should be modified. We set out with this project to detect possible temporal changes in the isotopic composition, but we find that such changes are not clearly quantifiable with the present analytical precision. Therefore the conclusion is a bit negative (as presented in the abstract), but have described our results and the limitations more quantitatively in the revised version.

Reply to Anonymous referee comments

Major comments:

Ref. Com. 1: Box model calculation: The model parameters that kept in varying are not stated clearly. A table that list all time independent parameteres (cross-tropopause exchange fluxes of isotopologues, natural fluxes and their associated isotopic signatures, N₂O lifetime, etc) will be helpful. In addition, a comparison with AR5 fluxes is useful.

Ref. Com. 2: Also box model: the derived time dependent variables. A table that summarizes the derived fluxes and isotopic values (average over a certain period) will be helpful, along with comparisons with other independent work by, for example, Park et al. and AR5.

Author's response to major comments 1 and 2:

We realise that a more detailed presentation of the parameters used is needed therefore we have substituted Table 3 where only natural and anthropogenic isotopic signature results were presented with a more detailed version including stratospheric loss fluxes and isotopic signatures, N₂O lifetime, natural and anthropogenic fluxes as in the two-box model. The values were compared to Park et al. (2012) because they provide results not only for fluxes but also for isotopic signatures. We did not include a comparison with the AR5 for the reason that it provides us only with flux results not isotopic signature ones.

Author's changes: Lines 989-995

Ref. Com. 3: What's the reason(s) behind for the elevated N₂O flux in year 2008?

Author's Resp.: We suspect the referee refers to the very slightly increasing emission strength at the end of the reconstructed record. This apparent upwards trend is likely not significant for our construction and we have not discussed it in more detail. We shortly stated this in the revised manuscript.

Author's changes: Lines 478-480

Ref. Com.4: *What's the reason(s) for the oscillating values in source/anthropogenic delta values in Fig. 4? Moreover, if I understand correctly, natural N₂O's are kept constant. I then expect to see the same time variability in anthropogenic as in source in Figure 4, but apparently the two are different. This highlights the usefulness of the major comment #1.*

Author's Resp.: The reason why the oscillations of the total and the anthropogenic source are not the same is that in our mass balance model the total source is regarded as the sum of a constant natural source and a changing anthropogenic source, which was small in the beginning of the record and larger at the end of the record. Therefore, changes in the total source signature in the beginning of the record require a substantially stronger isotope signal in the (small) anthropogenic source at that time compared to the (large) anthropogenic source at the end of the record. This was also stated in the manuscript. To make this more comprehensive we have added in Fig. 3 (bottom panel) the assumed constant, natural source, also.

Author's changes: Lines 515-520, Lines 1019-1037

Ref. Com. 5: *In addition to isotopic values, it will be useful and more informative to have isoflux for each process considered. A plot similar Fig. 4 but for the respective flux (better also break into each process considered is recommended).*

Author's Resp.: We have considered adding isofluxes to the manuscript, but since we only distinguish between a natural and an anthropogenic source this does not seem to add very useful information in our opinion. If – as the referee suggested – we were able to distinguish different processes it would indeed be useful, but since we cannot do that, we prefer not to add a discussion on isofluxes.

Minor comments:

Ref. Com. 1 section 2.5: *define all the variables used and no need to define variables not used. For example F_{sink} defined but not used. F_{exch} used but not defined. Also is epsilon_L the same as epsilon_app? Please check carefully the variables in this section.*

Author's Resp.: The section has been updated, F_{sink} is replaced by L, epsilon_L is not the same as epsilon_app. Epsilon_L is constrained by epsilon_app but the numerical values differ depending on F_{exch} and the lifetime. F_{exch} is defined in Table 3.

Author's changes: Lines 295-296, Lines 317-318, Line 320-321, Lines 989-995

Ref. Com. 2: *Line 445: additional decadal variability: raised also above in the major comment #4. What are the underlying mechanisms for the variability? Agricultural activity? Use of fertilizer?*

Author's Resp.: Yes these are the mechanisms we describe and we added some more clarification in the discussion section.

Author's changes: Lines 621-637

Ref. Com. 3: *Line 492: d₁₅N_{av}" is the same notation throughout, in the figure d₁₅N is used.*

Author's Resp.: The notation d15N in the figure was replaced with d15Nav.

Author's changes: Line 26, Line 32, Line 69, Line 70, Line 164, Line 166, Line 167, Line 170, Line 216, Line 224, Line 238, Line 247, Line 315, Line 414, Line 416, Line 430, Line 450, Line 494, Line 498, Line 501, Line 506, Line 520, Line 521, Line 522, Line 527, Line 537, Line 538, Line 544, Line 607, Line 629, Line 640, Line 697, Line 703, Line 708, Line 972-973, Line 991-995, Line 1029, Line 1058, Line 1134, Line 1136, Line 1172, Line 1197

Ref. Com. 4: *Line 495: Fig.5, I believed you meant Fig. 4. Do the corrections for the remaining.*

Author Resp.: Thank you for pointing this out, it has been corrected.

Ref. Com. 5: *Table 3: Is your delta_atm,pi the same as Park et al.? If not, why not compare? If the same then say it.*

Author's Resp.: The delta_atm,pi is the same as Park et al. and it is mention in the footnote denoted with an asterisk located below table 3.

Author's changes: Lines 992-995

Ref. Com. 6: *Same table, the last column double asterisk: what is it for?*

Author's Resp.: Thanks for noting this, the double asterisks was removed.

Ref. Com. 7: *Line 604: d15N_sp: not defined. You mentioned in line 36, but the term not defined.*

Author's Resp.: d15N_sp is now defined in line 37.

Author's changes: Line 37

Ref. Com. 8: *d15N_sp is useful: please also show the time series in Fig. 4*

Author's Resp.: The information has been added in the revised manuscript.

Author's changes: Lines 1029-1034

1 **Constraining N₂O emissions since 1940 using firn air isotope measurements in**
2 **both hemispheres**

3 **M. Prokopiou¹, P. Martinerie², C. J. Sapart^{1,3}, E. Witrant⁴, G. Monteil^{1,5}, K.**
4 **Ishijima⁶, S. Bernard², J. Kaiser⁷, I. Levin⁸, T. Blunier⁹, D. Etheridge¹⁰, E.**
5 **Dlugokencky¹¹, R. S. W. van de Wal¹, T. Röckmann¹**

6 ¹ Institute for Marine and Atmospheric research Utrecht, Utrecht, The Netherlands

7 ² University of Grenoble Alpes/CNRS, IRD, IGE, F-38000 Grenoble, France

8 ³ Laboratoire de Glaciologie, ULB, Brussels, Belgium

9 ⁴ University of Grenoble Alpes/CNRS, GIPSA-lab, F-38000 Grenoble, France

10 ⁵ Department of Physical Geography and Ecosystem Science, Lund University, Lund, Sweden

11 ⁶ National Institute of Polar Research, Tokyo, Japan

12 ⁷ Centre for Ocean and Atmospheric Sciences, School of Environmental Sciences, University
13 of East Anglia, Norwich, United Kingdom

14 ⁸ Institute of Environmental Physics, Heidelberg University, Germany

15 ⁹ Centre for Ice and Climate, Niels Bohr Institute, Copenhagen, Denmark

16 ¹⁰ CSIRO Marine and Atmospheric Research, Victoria, Australia

17 ¹¹ NOAA Earth System Research Laboratory, Boulder, Colorado, USA

18 **Abstract**

19 N₂O is currently the 3rd most important anthropogenic greenhouse gas in terms of radiative
20 forcing and its atmospheric mole fraction is rising steadily. To quantify the growth rate and its
21 causes over the past decades, we performed a multi-site reconstruction of the atmospheric
22 N₂O mole fraction and isotopic composition using new and previously published firn air data
23 collected from Greenland and Antarctica in combination with a firn diffusion and
24 densification model. The multi-site reconstruction showed that while the global mean N₂O
25 mole fraction increased from (290±1) nmol mol⁻¹ in 1940 to (322±1) nmol mol⁻¹ in 2008 the
26 isotopic composition of atmospheric N₂O decreased by (−2.2±0.2) ‰ for δ¹⁵N^{av}, (−1.0±0.3)
27 ‰ for δ¹⁸O, (−1.3±0.6) ‰ for δ¹⁵N^α, and (−2.8±0.6) ‰ for δ¹⁵N^β over the same period. The
28 detailed temporal evolution of the mole fraction and isotopic composition derived from the
29 firn air model was then used in a two-box atmospheric model (comprising a stratospheric and

30 a tropospheric box) to infer changes in the isotopic source signature over time. The precise
31 value of the source strength depends on the choice of the N₂O lifetime, which we choose to be
32 123⁺²⁹₋₁₉ a. The average isotopic composition over the investigated period is $\delta^{15}\text{N}^{\text{av}} =$
33 $(-7.6 \pm 0.8) \text{‰}$ (vs. air-N₂) $\delta^{18}\text{O} = (32.2 \pm 0.2) \text{‰}$ (vs. VSMOW) for $\delta^{18}\text{O}$, $\delta^{15}\text{N}^{\alpha} = (-3.0 \pm 1.9)$
34 ‰ and $\delta^{15}\text{N}^{\beta} = (-11.7 \pm 2.3) \text{‰}$. $\delta^{15}\text{N}^{\text{av}}$ and $\delta^{15}\text{N}^{\beta}$ show some temporal variability while for
35 the other signatures the error bars of the reconstruction are too large to retrieve reliable
36 temporal changes. Possible processes that may explain trends in ¹⁵N are discussed. The ¹⁵N
37 site-preference ($= \delta^{15}\text{N}^{\alpha} - \delta^{15}\text{N}^{\beta}$) provides evidence for a shift in emissions from
38 denitrification to nitrification, although the uncertainty envelopes are large.

39 1 Introduction

40 The rise of nitrous oxide (N₂O) since pre-industrial times contributes significantly to radiative
41 forcing (Forster et al., 2007). Over the past four decades, the N₂O mole fraction has increased
42 by 0.25 % per year, reaching 324 nmol mol⁻¹ in 2011 (Ciais et al., 2013). Therefore, the
43 understanding of the biogeochemical cycle of N₂O is important for a reliable assessment of
44 future climate change. In addition, the destruction of N₂O in the stratosphere provides an
45 important source of nitrogen oxides (NO_x), which contribute to stratospheric ozone depletion
46 (Ravishankara et al., 2009; Crutzen, 1979; McElroy et al., 1971).

47 Natural sources of N₂O are microbial processes in soils and oceans, which produce N₂O
48 during nitrification and denitrification (Bouwman et al., 2013; Loescher et al., 2012; Santoro
49 et al., 2011; Galloway et al., 2004; Pérez et al., 2001; Yung and Miller, 1997; Kim and Craig,
50 1993). The increase of N₂O since pre-industrial times (hereafter referred to as
51 "anthropogenic" increase) has been attributed largely to increased microbial production,
52 resulting from the increased use of nitrogen fertilizers in agriculture. Industry (especially
53 nylon production) and fossil fuel combustion present a smaller contribution to the
54 anthropogenic source (Davidson, 2009; Kroeze et al., 1999; Mosier et al., 1998). N₂O is
55 primarily destroyed in the stratosphere via UV photolysis (90 %) and reactions with excited
56 oxygen atoms (10 %) (Minschwaner et al., 1993), with a minor N₂O fraction removed by
57 surface sinks (Syakila, 2010).

58 Estimates of the total N₂O source strength from various bottom-up and top-down studies
59 suggest a mean value of roughly 17 Tg a⁻¹ N equivalents at present. However, the range in
60 both approaches is large, especially for bottom-up estimates, which range between 8.5 and
61 27.7 Tg a⁻¹ N, whereas top-down estimates range between 15.8 and 18.4 Tg a⁻¹ N (Potter et

62 al., 2011 and references therein). Besides the total source strength, the contributions of
63 individual source processes are also poorly constrained. Due to the long steady-state lifetime
64 of N₂O in the atmosphere (123₋₁₉⁺²⁹ a; SPARC Lifetimes Report 2013), temporal and spatial
65 gradients are small, making it difficult to resolve localised sources.

66 Measurements of the isotopic composition of N₂O may help to constrain the atmospheric N₂O
67 budget. The N₂O molecule is linear (NNO) and the two N atoms are chemically
68 distinguishable as a consequence they tend to attain different isotopic compositions. Beyond
69 oxygen ($\delta^{18}\text{O}$, $\delta^{17}\text{O}$) and average $\delta^{15}\text{N}^{\text{av}}$ ("bulk") signatures, N₂O also displays site specific
70 ¹⁵N isotopic information. Site preference ($\delta^{15}\text{N}^{\text{sp}}$) is defined as the difference in $\delta^{15}\text{N}^{\text{av}}$
71 between the central (2, μ or α) and terminal position (1, τ or β) of N atoms in N₂O (Kaiser,
72 2002; Brenninkmeijer and Röckmann, 2000; Yoshida and Toyoda, 1999), i.e. $\delta^{15}\text{N}^{\text{sp}} = \delta^{15}\text{N}^{\alpha} -$
73 $\delta^{15}\text{N}^{\beta}$. For consistency with many recent publications in the field, we here adopt the
74 nomenclature from Yoshida and Toyoda (1999), α and β , for the two positions.

75 The different sources and sinks of N₂O are associated with characteristic fractionation
76 processes leading to different isotope ratios. For example, microbial sources emit N₂O that is
77 depleted in ¹⁵N and ¹⁸O relative to the tropospheric background. N₂O that returns from the
78 stratosphere after partial photochemical removal is enriched in both heavy isotopes (Yoshida
79 and Toyoda, 2000; Rahn and Wahlen, 1997; Yung and Miller, 1997; Kim & Craig, 1993).
80 Stratospheric N₂O also has a high ¹⁵N site-preference compared to tropospheric N₂O. The
81 observed enrichment is caused by kinetic isotope fractionation in the stratospheric sink
82 reactions (Kaiser et al., 2006; 2002; Park et al., 2004; Röckmann et al., 2001; Yoshida and
83 Toyoda, 2000; Rahn et al., 1998).

84 The multi-isotope signature of N₂O adds useful constraints on its budget. In particular, when
85 the isotopic composition of tropospheric N₂O is combined with the fractionation during its
86 removal in the stratosphere, the isotopic composition of the global average source can be
87 determined (Ishijima et al., 2007; Bernard et al., 2006; Röckmann et al., 2003; Kim and Craig,
88 1993).

89 The temporal variations of the N₂O isotopic composition are difficult to quantify on a short
90 timescale because of its long residence time in the atmosphere. Longer time scales can be
91 reconstructed by using air trapped in Arctic and Antarctic firn and ice which provides a
92 natural archive of past atmospheric composition. The firn phase is the intermediate stage
93 between snow and glacial ice, which constitutes the upper 40-120 m of the accumulation zone

94 of ice sheets. Within the firn, air exchanges relatively freely in the upper layers and with the
95 overlying atmosphere (convective zone). With increasing depth the air pores shrink in size
96 due to firn compaction, and air mixes primarily via slow diffusion in the diffusive zone. At
97 densities larger than $\approx 815 \text{ kg m}^{-3}$, air is permanently trapped in closed bubbles in the ice and
98 totally isolated from the atmosphere. The precise age range of air that can be retrieved from
99 polar firn between the surface and bubble close-off depends on site specific characteristics
100 like temperature, accumulation rate and porosity and typically ranges from several decades to
101 120 years.

102 For N_2O , a number of studies have reported isotope measurements from different Arctic and
103 Antarctic firn drilling sites showing a steady decrease of the heavy isotope content of N_2O
104 over the past decades (Park et al., 2012; Ishijima et al., 2007; Bernard et al., 2006; Röckmann
105 et al., 2003; Sowers et al., 2002). A more recent study by Park et al. (2012) attempted to
106 reconstruct the long-term trends in N_2O isotopic compositions and its seasonal cycles to
107 further distinguish between the influence of the stratospheric sink and the oceanic source at
108 Cape Grim, Tasmania, demonstrating that isotope measurements can help in the attribution
109 and quantification of surface sources in general.

110 Taking into account the long atmospheric lifetime of N_2O and the fact that both hemispheres
111 are well mixed on annual timescales, it is reasonable to assume that the results from these
112 studies are representative for the global scale. However care needs to be taken because small
113 differences in the diffusivity profiles of the firn column lead to large effect on the isotope
114 signature (Buizert et al., 2012). Interestingly, for atmospheric methane (CH_4), another
115 important greenhouse gas, a recent multi-site analysis of its carbon isotopic composition
116 showed large differences among reconstructions from different sites (Sapart et al., 2013). In
117 particular, firn fractionation effects related to diffusion and gravitational separation and their
118 implementation in models (Buizert et al., 2012) have large effects on the reconstructed
119 signals. Small differences in the diffusivity profiles of the firn column lead to large effects on
120 the isotope signatures. Therefore, more robust results may be obtained by combining isotope
121 information from a number of different sites in a multi-site reconstruction, including a critical
122 evaluation of diffusivity profiles.

123 Here we combine new N_2O isotope measurements from the NEEM site in Greenland with
124 previously published firn air N_2O isotope records from 4 different sites from Greenland and
125 Antarctica to reconstruct records of the N_2O isotopic composition over the last 70 years. We

126 use the multi-gas firn transport model developed by the Laboratoire de Glaciologie et
127 Géophysique de l'Environnement and Grenoble Image Parole Signal Automatique (LGGE-
128 GIPSA) to obtain an atmospheric scenario that is constrained by and consistent with all
129 individual sites (Allin et al., 2015; Witrant et al., 2012; Wang et al., 2012; Rommelaere et al.,
130 1997). We then use an isotope mass balance model to infer the changes in the isotopic
131 signature of the N₂O source over time to investigate possible changes in the source mix.

132 **2 Materials and Methods**

133 **2.1 Firn air Sampling**

134 New firn air samples added in this study to the total dataset were collected in 2008 and 2009
135 during the firn campaign (Buizert et al., 2011) as part of the North Eemian Ice Drilling
136 programme (NEEM) in Greenland (77.45° N 51.06° W). These data are combined with
137 existing firn air data from four other sites. Information on the locations is provided in Table 1.
138 The firn air collection procedure is described in detail by Schwander et al. (1993). Here a
139 brief description is presented. Essentially a borehole is drilled in the firn to a certain depth and
140 then the firn air sampling device is inserted into the borehole. The device consists of a
141 bladder, a purge line and a sample line. When the sampling device reaches the desired depth
142 the bladder is inflated to seal the firn hole and isolate the air below the bladder from the
143 overlying atmosphere, and air is pumped out from the pore space below the bladder.
144 Continuous online CO₂ concentration measurements are performed to verify that no
145 contamination with contemporary air occurs during the extraction procedure. After the
146 contaminating air has been pumped away, firn air is collected in stainless steel, glass or
147 aluminium containers.

148 **2.2 N₂O isotope analysis**

149 The firn air samples from NEEM are analyzed for N₂O isotopocules at the Institute for
150 Marine and Atmospheric research Utrecht (IMAU). The N₂O mole fraction and isotopic
151 composition are measured using continuous flow isotope ratio mass spectrometry (IRMS).
152 The method is described in detail by Röckmann et al. (2003b). Here only a brief summary is
153 given. The firn air sample (333 mL) is introduced into the analytical system at a flow rate of
154 50 mL/min for 400 s. After CO₂ is removed chemically over Ascarite, N₂O and other
155 condensable substances are cryogenically preconcentrated. After cryo-focusing the sample the

156 remaining traces of CO₂ and other contaminants are removed on a capillary GC column
157 (PoraPlot Q, 0.32 mm i.d., 25 m). The column is separated into a pre-column and an
158 analytical column. This set-up eliminates interferences from other atmospheric compounds
159 that have much longer retention times. Finally the sample is transferred to the IRMS via an
160 open split interface. For the new NEEM samples reported here, each firn air sample has been
161 measured five times. Before and after each sample we measured five aliquots of air from a
162 reference cylinder with known isotopic composition and mole fraction for calibration
163 purposes.

164 $\delta^{15}\text{N}^{\text{av}}$ values are reported with respect to Air-N₂ while $\delta^{18}\text{O}$ refers to Vienna Standard Mean
165 Ocean Water (VSMOW). As laboratory reference gas we used an atmospheric air sample with
166 an N₂O mole fraction of 318 nmol mol⁻¹ and δ values of (6.4±0.2) ‰ for $\delta^{15}\text{N}^{\text{av}}$ vs. Air-N₂,
167 (44.9±0.4) ‰ for $\delta^{18}\text{O}$ vs. VSMOW. The intramolecular $\delta^{15}\text{N}^{\text{av}}$ values of the air standard are
168 $\delta^{15}\text{N}^{\alpha} = (15.4\pm 1.2)$ ‰ and $\delta^{15}\text{N}^{\beta} = (-2.7\pm 1.2)$ ‰. The calibration of the intramolecular
169 distribution follows Toyoda and Yoshida (1999). Typically the 1 σ standard deviations of
170 replicate sample measurements are 0.1 ‰ for $\delta^{15}\text{N}^{\text{av}}$, 0.2 ‰ for $\delta^{18}\text{O}$ and 0.3 ‰ for $\delta^{15}\text{N}^{\alpha}$ and
171 $\delta^{15}\text{N}^{\beta}$.

172 **2.3 Modelling trace gas transport in firn**

173 In firn air, the interstitial gas is not yet isolated in closed-off bubbles, so diffusion processes
174 and gravitational separation alter mole fractions and isotope ratios over time. Thus, firn air
175 measurements cannot be used directly to derive the atmospheric history of trace gas
176 signatures. Over time, atmospheric compositional changes are propagated downwards into the
177 firn based on the diffusivity of the atmospheric constituent in question. Firn air diffusion
178 models take these effects into account and thereby allow reconstruction of changes in the
179 atmospheric composition from the firn profile.

180 In this study we use the LGGE-GIPSA firn air transport model to reconstruct the temporal
181 evolution of N₂O mole fraction and isotopic composition from the measured firn profiles
182 (Allin et al., 2015; Witrant et al., 2012; Wang et al., 2012; Rommelaere et al., 1997).

183 In the “forward version” of LGGE-GIPSA, a physical transport model uses a historic
184 evolution of atmospheric N₂O mole fractions to calculate the vertical profiles of mole
185 fractions in firn. For the isotopocules, further simulations are performed separately to
186 calculate their respective vertical profiles. Important parameters needed to constrain the

187 model are the site temperature, accumulation rate, depth of the convective layer and close-off
188 depth, together with profiles of firn density and effective diffusivity. The latter parameter is
189 determined as a function of depth for each firn-drilling site by modelling the mole fractions in
190 firn for trace gases with well known atmospheric histories (Buizert et al., 2012; Witrant et al.,
191 2012; Rommelaere et al., 1997; Trudinger et al., 1997). A multi-gas constrained inverse
192 method (Witrant et al., 2012) is used to calculate the effective diffusivity of each site for each
193 specific gas. It is noteworthy that diffusivity is not constrained equally well at all sites
194 because different sets of constraints (e.g. number of available reference gases) are used at
195 different sites and because of different depth resolutions.

196 A Green-function approach, as presented by Rommelaere et al. (1997) and used for
197 halocarbon trend reconstruction by Martinerie et al. (2009), with an extension for isotopic
198 ratios and revised to take into account the scarcity of the measurements (Allin et al., 2015;
199 Witrant and Martinerie, 2013; Wang et al., 2012) is used to assign a mean age and age
200 distribution to a certain depth.

201 Due to the long N₂O residence time in the atmosphere, the global variability of the isotopic
202 composition of N₂O is very small and no significant variations between individual
203 background locations have been detected so far (Kaiser et al., 2003). In particular, the isotope
204 ratio difference between northern and southern hemisphere tropospheric air is expected to be
205 only -0.06 ‰ (based on an interhemispheric mole fraction gradient of 1.2 nmol mol^{-1} [Hirsch
206 et al. 2006] and isotope ratio difference of -15 ‰ between average source and average
207 tropospheric isotopic delta value). These differences are within the uncertainties of the firn air
208 measurements used here and therefore the data from the northern and southern hemisphere are
209 combined into a single dataset without including an interhemispheric gradient.

210 With the multi-site reconstruction method, we used the measurements from six firn air
211 drillings at five sites (NEEM-09, NEEM-EU-08, BKN-03, NGRIP-01_{Bernard}, DC-99, DML-
212 98) to constrain our model and determine a set of atmospheric reconstructions that fits all
213 sites. Data from Ishijima et al. (2007) and Sowers et al. (2002) [NGRIP-01_{Ishijima} and SP-01,
214 SP-95 respectively] were not included in our multi-site reconstruction because no data for
215 $\delta^{15}\text{N}^{\alpha}$ and $\delta^{15}\text{N}^{\beta}$ were published for those sites. These datasets were used for independent
216 validation of $\delta^{15}\text{N}^{\text{av}}$ and $\delta^{18}\text{O}$.

217 To quantify the isotope fractionation due to diffusion and gravitational settling within the firn,
218 a forward firn transport model simulation was carried out with a realistic N₂O mole fraction

219 scenario (based on the Law Dome record, MacFarling Meure et al., 2006), but with a constant
220 isotopic N₂O history. This allows determining the role of transport isotope fractionation
221 occurring in the firn, in the absence of isotopic changes in the atmosphere. The results are
222 used to subtract the firn fractionation effects from the measured signals, which can then be
223 used to assess the atmospheric history. Compared to the signal, the effect of firn fractionation
224 is minor for $\delta^{15}\text{N}^{\text{av}}$, but important for $\delta^{18}\text{O}$ especially at the lower accumulation rates in the
225 Southern Hemisphere (see Appendix A).

226 The deepest firn data from each site provide constraints furthest back in time and the oldest
227 air samples that are included in the inversion are from the DML-98 and DC-99, which extend
228 the reconstruction of atmospheric N₂O back to the early 20th century (Röckmann et al., 2003).
229 At the same time, the correction for isotopic fractionation in firn is most uncertain for the
230 deepest samples, where strong differences between individual firn air models have been
231 reported (Buizert et al., 2012).

232 **2.4 Scaling of different data sets**

233 At present, no international reference materials for the isotopic composition of N₂O exist.
234 Kaiser et al. (2003) and Toyoda et al. (1999) linked the isotopic composition of N₂O in
235 tropospheric air to the international isotopes scales for nitrogen isotopes (Air-N₂) and oxygen
236 isotopes (either VSMOW or Air-O₂). Our measurements are linked to a standard gas cylinder
237 of tropospheric air with known N₂O mole fraction and isotopic composition based on the
238 scale of Kaiser et al. (2003) for $\delta^{15}\text{N}^{\text{av}}$ and $\delta^{18}\text{O}$ values and Yoshida and Toyoda (1999) for
239 position dependent ¹⁵N values. However, the reference air cylinder used for the calibration
240 was exhausted and had to be replaced three times over the years in which the different
241 measurement that we combine in this study were performed. Although the cylinders were
242 carefully compared, the long-time consistency of the isotope scale could not be guaranteed
243 because long-time isotope standards are not available. In fact, analysis of the data from the
244 convective zone for the different sites, show small but significant differences from the
245 temporal trends that are well established from previously published data from the German
246 Antarctic Georg von Neumayer station for 1990 to 2002 (Röckmann and Levin; 2005). The
247 linear trends reported in that paper are $(-0.040 \pm 0.003) \text{‰ a}^{-1}$ for $\delta^{15}\text{N}^{\text{av}}$, $(0.014 \pm 0.016) \text{‰ a}^{-1}$
248 for $\delta^{15}\text{N}^{\alpha}$, $(-0.064 \pm 0.016) \text{‰ a}^{-1}$ for $\delta^{15}\text{N}^{\beta}$ and $(-0.021 \pm 0.003) \text{‰ a}^{-1}$ for $\delta^{18}\text{O}$. Since they were
249 derived from direct air samples (unaffected by firn fractionation), these trends can be used as

250 a reference to re-scale the different firn air results from different dates. To do so, data from
251 the diffusive zone ($\rho < 815 \text{ kg m}^{-3}$) for each individual site were scaled to one reference site,
252 DC-99, taking into account the temporal differences in sampling and the model-assigned
253 mean age of the firn air samples (see below). DC-99 was chosen as reference site because it
254 has most measurements in the diffusive zone. Also, the precision of these measurements was
255 high because high volume cylinders were available from which many measurements could be
256 performed and averaged. To test the sensitivity to the choice of reference site, we repeated the
257 re-scaling using NEEM-09 as reference, which generated almost identical results within
258 uncertainty bars (Appendix C).

259 The average difference between the samples from the diffusive zone at a given site and the
260 interpolated DC-99 results was compared to the expected temporal trend between the
261 sampling date of each station and DC-99, using the temporal trends established by Röckmann
262 and Levin (2005), as shown in the equations below. The effect of this scaling is that the
263 temporal trend in the past decade is effectively forced to follow the atmospheric
264 measurements at Neumayer station (Röckmann and Levin, 2005).

265 After re-scaling the firn isotopic data we detected some individual data points that clearly
266 deviated from the general trends. These were considered outliers, because they exceeded the
267 2σ error, and were removed from the dataset. All of these values are site-specific ^{15}N values,
268 specifically the following, were excluded: NEEM-EU-08 hole depth -4.9 m , -34.72 m , $-$
269 61.95 m and -74.5 m , and NEEM-09 hole depth 1.0 m , 0.2 m and -69.4 m .

270 The mole fraction data that can be obtained from the NEEM air isotope measurements were
271 substituted with more precise measurements of N_2O mole fraction by the Commonwealth
272 Scientific and Industrial Research Organisation (CSIRO) the Institute of Environmental
273 Physics, University of Heidelberg (IUP), the Centre of Ice and Climate, University of
274 Copenhagen (CIC) and National Oceanic and Atmospheric Administration (NOAA). **In this
275 way we combine all available N_2O mole fraction data narrow the uncertainty envelope but do
276 not affect the trend.**

277 The mole fraction data were scaled to the most recent international scale, NOAA-2006A from
278 the CSIRO scale or the NOAA-2000 scale. Conversion of the NOAA-2000 data to the
279 NOAA-2006A scale is done using a conversion factor available by National Oceanic and
280 Atmospheric Administration (NOAA)
281 (http://www.esrl.noaa.gov/gmd/cc1/scales/N2O_scale.html). Converting from the CSIRO to

282 the NOAA-2006A scale, though, requires the reference cylinder details, which were not
 283 available. Instead we used a trend scenario, based on the CSIRO atmospheric scale combined
 284 with Law Dome data and assuming a constant interhemispheric gradient. This trend scenario
 285 was then compared with the data provided on NOAA-2006A scale, and a polynomial fit was
 286 generated, which was then used to convert the data to the NOAA-2006A scale. All results
 287 presented in the next section are based on the scaling procedure and removal of the outliers as
 288 described above (Appendix B).

289 **2.5 Global N₂O (isotope) budget calculations**

290 The tropospheric budget is controlled by N₂O emissions from natural and anthropogenic
 291 sources at the surface and by the exchange between troposphere and stratosphere. A simple
 292 two-box model is used to quantitatively understand the emissions and the budget changes of
 293 N₂O. The model consists of a tropospheric N₂O reservoir (index T) into which N₂O is emitted
 294 from natural (E_{nat}) and anthropogenic (E_{anth}) sources. N₂O is then transported to the
 295 stratosphere (index S) where part of it is destroyed by photochemical reactions (L), and the
 296 remainder returns from the stratosphere to the troposphere (F_{exch}).

297 The change in the tropospheric N₂O reservoir is given by the following mass balance
 298 equations (Allin et al, 2015):

$$299 \quad n_T \frac{d\chi_T}{dt} = E_{\text{nat}} + E_{\text{anth}} - F_{\text{exch}}(\chi_T - \chi_S) \quad (1)$$

$$300 \quad n_S \frac{d\chi_S}{dt} = F_{\text{exch}}(\chi_T - \chi_S) - L \quad (2)$$

301 where n is the amount of air and χ_S and χ_T are the mole fractions of N₂O in the stratosphere
 302 and troposphere respectively. Annual fluxes between the two reservoirs, F_{exch}, are calculated
 303 based on previous estimates (Appenzeller et al., 1996; Holton et al., 1990) and given in Table
 304 3. The loss due to stratospheric sink is determined by:

$$305 \quad L = \frac{n_T \chi_T + n_S \chi_S}{\tau} \quad (3)$$

306 where τ is the atmospheric lifetime of 123⁺²⁹₋₁₉ a.

307 The isotopic budgets are calculated by simply multiplying the reservoir sizes with the
 308 corresponding δ values of the different flux terms:

$$309 \quad n_T \frac{d\chi_T \delta_T}{dt} = E_{\text{nat}} \delta_{\text{nat}} + E_{\text{anth}} \delta_{\text{anth}} + F_{\text{exch}}(\chi_S \delta_S - \chi_T \delta_T) \quad (4)$$

$$310 \quad n_S \frac{d\chi_S \delta_S}{dt} = F_{\text{exch}}(\chi_T \delta_T - \chi_S \delta_S) - L \delta_L \quad (5)$$

311 Separating the l.h.s in two terms and substituting eq. 1 and 2 into eq. 4 and 5 yields the final
312 isotope equations:

$$313 \quad n_T \frac{d\delta_T}{dt} = \frac{E_{\text{nat}}}{\chi_T} (\delta_{\text{nat}} - \delta_T) + \frac{E_{\text{anth}}}{\chi_T} (\delta_{\text{anth}} - \delta_T) + \frac{F_{\text{exch}} \chi_S}{\chi_T} (\delta_S - \delta_T) \quad (6)$$

$$314 \quad n_S \frac{d\delta_S}{dt} = \frac{F_{\text{exch}} \chi_T}{\chi_S} (\delta_T - \delta_S) - \frac{L}{\chi_S} \varepsilon_L \quad (7)$$

315 where δ_T is either $\delta^{15}\text{N}^{\text{av}}$, $\delta^{18}\text{O}$, $\delta^{15}\text{N}^{\alpha}$, $\delta^{15}\text{N}^{\beta}$ from the multi-site reconstruction as shown
316 below. δ_{nat} and δ_{anth} is the isotopic composition of the natural and anthropogenic N_2O source,
317 respectively (our target quantity). ε_L is the apparent Rayleigh fractionation factor associated
318 with stratospheric destruction.

319 δ_S is also not known, but can be calculated using the analogue from Röckmann et al. (2003)
320 by employing the observed apparent Rayleigh fractionation in the stratosphere (ε_{app}) (Table
321 3). Based on this, the relative isotope ratio difference between the stratosphere and the
322 troposphere can be calculated by:

$$323 \quad \delta_S = \left[(\delta_T + 1) \left(\frac{\chi_S}{\chi_T} \right)^{\varepsilon_{\text{app}}} - 1 \right] \quad (8)$$

324 Here, we used the average ε_{app} of all lowermost stratospheric measurements from Kaiser et al.
325 (2006) (Table 3). Note that slightly different fractionations ε_{app} have been used in previous
326 studies by Rahn and Wahlen (2000), Röckmann et al. (2001) and Park et al. (2012; 2004). The
327 sensitivity of the results to these differences will be examined below.

328 Furthermore we assume that the N_2O lifetime and ε_{app} remained constant from pre-industrial
329 time to 2008, thus the annual sink strength can be scaled down from its current value at $\chi_T =$
330 322 nmol mol^{-1} to the pre-industrial level of $\chi_{T,\text{pi}} = 270 \text{ nmol mol}^{-1}$ and the relative enrichment
331 of stratospheric N_2O relative to tropospheric N_2O described by Eq. 8 remains constant over
332 time. The effect of changing the N_2O lifetime is also examined below.

333 Our model approach assumes that during the pre-industrial period only natural emissions
334 occurred without any anthropogenic input. After the industrialization (≈ 1750) any increase in
335 the emissions is considered to be due to anthropogenic input while natural emissions remain
336 constant. Hence, the temporal change in isotopic composition is formally due to the increase

337 in one single “anthropogenic” source only, which may in reality also contain a natural
338 component.

339 **2.6 Uncertainty estimation using random scenarios**

340 The precision of the calculated N₂O emissions (E_{nat} , E_{anth}) depends primarily on the precision
341 of the atmospheric reconstruction of the N₂O mole fraction (χ_T). However, taking random
342 histories within the uncertainty envelope provided by the firm air reconstruction is not
343 adequate to quantify the uncertainty of the atmospheric N₂O reconstruction: the year-to-year
344 variability of N₂O is constrained by the N₂O lifetime in the troposphere. Possible realistic
345 N₂O scenarios are scenarios that are within the confidence intervals provided by the
346 atmospheric reconstructions, and that have realistic year-to-year variability.

347 Mathematically, this can be represented by an uncertainty variance covariance matrix \mathbf{B} ,
348 where the diagonal elements (variances) are the yearly uncertainties on the atmospheric N₂O
349 mole fractions, and the off-diagonals are the covariances of the uncertainties of different
350 years. The covariance between the uncertainty on the reconstruction in one year i and the
351 uncertainty in another year j is defined as:

$$352 \quad \text{cov}(i,j)=r_{i,j}\sigma_i\sigma_j \quad (9)$$

$$353 \quad r_{i,j}=f(|i-j|) \quad (10)$$

354 The correlation ($r_{i,j}$) is maximum between two consecutive years, and decreases as the time
355 difference increases.

356 We generated an ensemble of 50 random realistic N₂O scenarios within the uncertainty
357 envelope of the firm atmospheric N₂O reconstruction constrained by the covariance matrix \mathbf{B} .
358 For each of these atmospheric N₂O scenarios, we calculated the corresponding N₂O emission
359 time series. The range of emissions from these scenarios then provides a realistic estimate for
360 the uncertainty in N₂O emissions.

361 We carried out the same analysis for the different N₂O isotopocules: for each isotopocule (δ
362 value), we generated a covariance matrix \mathbf{B}^δ , constrained by the uncertainty ranges provided
363 by the atmospheric reconstructions and the correlation coefficients defined in Eq.9 and Eq.10
364 to generate a set of 50 random scenarios within the uncertainty envelopes. For each of these

365 random scenarios, we calculated the corresponding source signature scenario and the range in
366 the results provides an uncertainty estimate of the isotopic source signatures.

367 **3 Results**

368 **3.1 Mean age**

369 The mean age of N₂O in air sampled from different depths in the firn for all datasets that are
370 used in this study is shown in Fig. 1. The strong change in the mean age gradient that is
371 clearly visible in each profile reflects the transition between the diffusive and bubble close-off
372 zones, which occurs at a specific depth and mean age for each site (marked with x on Fig. 1).
373 Fig. 1 also shows that for each site the few samples that are collected within the bubble close-
374 off zone provide the constraints for most of the reconstructed record (for instance, at BKN-03,
375 50 m depth is the beginning of the bubble close-off zone). In addition to the mean age, the
376 width of the age spectrum also increases with depth. Therefore, the temporal resolution of
377 signals that can be reconstructed from the firn air measurements reduces with depth and
378 approaches the one of ice core samples towards the bottom of the bubble close-off zone.

379 The Greenland sites (NH) have similar meteorological and glaciological conditions (Table 1),
380 thus the differences between the mean age profiles in Fig. 1 are small. The Antarctic sites
381 (SH) show clear differences because the meteorological and glaciological variables differ
382 strongly from site to site. As a result the firn-ice transition is at a different depth for each
383 location (e.g., the firn-ice transition zone for DML-98 is located at about 73.5 m compared to
384 about 99.5 m at DC-99).

385 **3.2 Experimental results and multi-site reconstruction**

386 Mole fraction and isotopic composition of N₂O in firn air are presented versus depth of the
387 firn air sampling in the middle panels of Fig. 2 for the different sites. The mole fraction
388 decreases with depth in qualitative agreement with the known increase of N₂O in the
389 atmosphere over time. In contrast, all isotope deltas slowly increase with depth in the upper
390 firn and show stronger heavy isotope enrichment in the close-off zone, both indicating heavy
391 isotope depletion in atmospheric N₂O with time.

392 The atmospheric history that has been reconstructed from these firn datasets using the multi-
393 site inversion (using the data from NEEM-09, NEEM-EU-08, NGRIP-01^{Bernard}, BKN-03, DC-
394 99, DML-98) as described in section 2.4 is shown in the left column of Fig. 2. The solid line

395 shows the scenario that leads to the best fit with the firm data as shown in the middle panel,
396 and the dashed lines show the upper and lower range of possible scenarios that would still
397 produce an acceptable fit to the data within the uncertainty bars. Color-coded symbols show
398 data plotted at their respective mean age (as derived from the firm air model). When the best-
399 fit scenario is used as input for the forward firm air model for each individual site, the model
400 produces the vertical profiles that are shown as coloured lines together with the data in the
401 middle panels. For the sites that were included in the multi-site reconstruction, the firm
402 profiles based on the best-fit scenarios generally match the experimental data points well,
403 which is expected after a successful inversion procedure and with consistent data sets. The
404 right panels in Fig. 2 show the differences between these model results and the data. For the
405 data that were used in the multi-site inversion the model-data differences are generally very
406 small, although individual firm drilling sites in some cases show small systematic deviations,
407 in particular in the close-off zone. This means that when inversions would have been
408 performed on individual sites, the optimal reconstructions would be slightly different. Hence,
409 the advantage of the multi-site reconstruction is that the reconstructed scenario is constrained
410 by all sites and all sampling depths. Despite the small differences between individual sites, the
411 left panels show that all data fall within the uncertainty bars of the reconstructed scenario of
412 the inversion.

413 From 1940 to 2008 the total changes of the δ values of atmospheric N_2O are $(-2.2 \pm 0.2) \text{ ‰}$ for
414 $\delta^{15}N^{Tav}$, $(-1.0 \pm 0.3) \text{ ‰}$ for $\delta^{18}O$, $(-1.3 \pm 0.6) \text{ ‰}$ for $\delta^{15}N^a$ and $(-2.8 \pm 0.6) \text{ ‰}$ for $\delta^{15}N^b$
415 respectively (Fig. 2, left panels). The average linearized trends are $(-0.032 \pm 0.004) \text{ ‰ a}^{-1}$ for
416 $\delta^{15}N^{Tav}$, $(-0.014 \pm 0.008) \text{ ‰ a}^{-1}$ for $\delta^{18}O$, $(-0.019 \pm 0.015) \text{ ‰ a}^{-1}$ for $\delta^{15}N^a$ and (-0.041 ± 0.020)
417 ‰ a^{-1} for $\delta^{15}N^b$. These overall trends are slightly lower compared to previous studies that
418 used only the data at individual sites (Ishijima et al., 2007; Bernard et al., 2006; Röckmann et
419 al., 2003; Sowers et al., 2002) and other studies that used data from the same period, which
420 were not used in the present study (Park et al., 2012). However, the differences are well
421 within the combined uncertainties. We note that comparisons of average linear trends can be
422 flawed when the firm air records have different length and the temporal profiles do not change
423 linearly (see below). Trends for $\delta^{15}N^a$ are smaller in magnitude than for $\delta^{15}N^b$, while results
424 from Bernard et al. (2006) showed stronger changes for $\delta^{15}N^a$ than for $\delta^{15}N^b$. However, in that
425 study the trends were largely determined from measurements on young ice core samples with
426 comparatively higher measurement errors and larger scatter.

427 Data from two sites were not included in the multi-site inversion and are used as independent
428 validation of the reconstructed scenarios. The data points from Ishijima et al. (2007) (NGRIP-
429 01_{Ishijima}, yellow) are within the range of scenarios reconstructed by the inverse model and
430 thus independently validate our results. The $\delta^{15}\text{N}^{\text{av}}$ and $\delta^{18}\text{O}$ data from Sowers et al. (2002)
431 (SP-01 in light blue and SP-95 in blue) however, agree only for the more recent atmospheric
432 history (Fig. 2, left panels). For mean ages before 1990 most of the points are outside the
433 uncertainty envelopes of the multi-site reconstruction. Inter-laboratory calibration differences
434 might be a possible explanation for the discrepancy, but the differences are not a systematic
435 shift, and they are larger than offsets among laboratories that were established in the past
436 (Sapart et al., 2011; Kaiser et al., 2003). In fact, the data reported by Sowers et al. (2002)
437 were actually measured in two different laboratories with good agreement. So measurement
438 flaws can be excluded. A possible origin of the difference could be based on the
439 reconstruction model. Because the uncertainties on the South Pole data are large, compared to
440 the other sites, the multi-site homogenization is more uncertain and less efficient (see
441 Appendix A and C, Fig. A1 and C1-C3). Sampling uncertainty should also be taken into
442 consideration since when pumping firm air and filling the sampling flasks you could encounter
443 uncertainties (contamination, possible leak, fractionation, incomplete flask flushing etc). At
444 present though the discrepancy cannot be resolved.

445 To evaluate our scaling approach we repeated the multi-site reconstruction using the original
446 non re-scaled data and re-scaled them to NEEM-09 instead of DC-99 (see Appendix C). This
447 yielded similar results (within uncertainties) to the original reconstruction, thus results do not
448 depend on the choice of the site used for re-scaling. Without re-scaling, the overall change of
449 N_2O mole fraction and isotopic composition remained the same, but an additional decadal
450 variability was introduced for $\delta^{15}\text{N}^{\text{av}}$, $\delta^{15}\text{N}^{\alpha}$ and $\delta^{15}\text{N}^{\beta}$. In addition to that, the uncertainty
451 envelopes doubled because of the scale inconsistencies. All scaling approaches produce
452 results that are consistent with our preferred scaling to DC-99 within the uncertainty
453 envelopes. We conclude that scaling removed the discrepancies that would cause larger
454 uncertainties if the original data were used instead, but the re-scaling does not introduce
455 artificial signals (see Appendix C).

456 The regularization of the inversion results using a rugosity factor introduces a free parameter,
457 which is chosen to eliminate overfitting of experimental uncertainties and which controls the
458 smoothness of the reconstruction. The value of this parameter is set based on a robust

459 generalized cross validation criterion, ensuring that the resolution obtained from the inverse
460 model is similar to the experimental data while taking into account the scarcity of the
461 measurements (Witrant and Martinerie, 2013). A sensitivity experiment where the weight of
462 the regularization term was increased by a factor 10 led to nearly linear tropospheric histories
463 within the uncertainty envelopes presented in Appendix C (Fig. C2). This combined with the
464 fact that straight lines can be drawn within the uncertainty envelopes of the reconstructed
465 scenarios and the sensitivity tests (see Appendix C) indicates that the isotopic trends are not
466 significantly different from straight lines within the current uncertainties.

467 **3.3 Reconstruction of the N₂O emission history**

468 Fig. 3 shows the temporal evolution of the global N₂O mole fraction as inferred from the
469 atmospheric reconstruction constrained only by the most precise NEEM data in the top panel,
470 and in the bottom panel the emission strength in Tg a⁻¹ N calculated with the mass balance
471 model (Section 2.5). The solid black line denotes the best estimate scenario, which is used as
472 input in the mass balance model. The magenta lines show the ensemble of random scenarios
473 generated to quantify the uncertainty of the emissions (see Section 2.6).

474 The increase in the N₂O mole fraction of (32±1) nmol mol⁻¹ over the reconstruction period
475 can be explained in the mass balance model by a (4.4±1.7) Tg a⁻¹ N increase in the emissions
476 from 1940 to 2008. The emissions increased with an increasing trend until 1975, then the
477 annual increase continued, but at a slower rate up to 1990, and from then on the annual
478 emissions have stayed approximately constant or even decreased slightly. The minor increase
479 in the N₂O mole fraction towards the end of the time series is likely not significant and does
480 influence our reconstructions. The corresponding changes in the mole fraction are difficult to
481 discern due to the long atmospheric lifetime of N₂O. On average, the annual growth rate from
482 1995 to 2008 period is 0.7 nmol mol⁻¹ a⁻¹, corresponding to average annual emissions of 3.5
483 Tg a⁻¹ N.

484 **3.4 The temporal evolution of the N₂O isotope signatures**

485 The results from the isotope budget calculations are presented in Fig. 4. The left panels show
486 the atmospheric trends. The solid black lines represent the best-fit scenarios while the dashed
487 black lines represent the upper and lower uncertainty envelope of the firm air reconstructions.
488 The magenta lines represent 50 scenarios generated randomly within the reconstructed
489 uncertainty range, as described in section 2.6. The middle panels show the temporal changes

490 in the isotope signatures of the total N₂O source, with their accompanied uncertainties, as
491 calculated from the atmospheric mass balance model (section 2.5). The total source is split
492 into an assumed constant "natural" and an increasing "anthropogenic" component and the
493 right panels show the isotopic evolution of the "anthropogenic" component.

494 Results show that the average $\delta^{15}\text{N}^{\text{av}}$ of the total N₂O source, over the reconstruction period, is
495 (-7.6 ± 0.6) ‰ where the uncertainty is calculated using the 1σ uncertainty from the scenarios
496 with respect to the mean value (magenta lines). There is no statistically significant long-term
497 trend, but a temporal variability is observed on the decadal scale that might mask this trend.
498 $\delta^{15}\text{N}^{\text{av}}$ first decreased from (-6.5 ± 0.6) ‰ in 1940 to (-8.5 ± 0.6) ‰ in 1965, then slowly
499 increased again to (-6.6 ± 0.6) ‰ in 1985, followed by another decrease to (-8.5 ± 0.6) ‰ in
500 2008. These oscillations originate from the slightly curved trends in the isotopic
501 reconstructions for $\delta^{15}\text{N}^{\text{av}}$ in Fig. 4 (left panels).

502 When the source is split into a constant natural and a varying anthropogenic component, the
503 variability is projected on the anthropogenic part and the temporal variations increase
504 accordingly. However, also the uncertainties increase substantially, because the differences
505 between the individual scenarios are attributed to only a small fraction of the total source.

506 The $\delta^{15}\text{N}^{\text{av}}$ signature of the anthropogenic source has an average value of (-18.2 ± 2.6) ‰. It
507 initially increases (the small initial decrease is not significant) from (-21.5 ± 2.6) ‰ in 1940 to
508 (-8.6 ± 2.6) ‰ in 1990, when it starts to slowly decrease reaching (-15.4 ± 2.6) ‰ in 2008.
509 During the early part of the reconstruction period before 1970, when the "anthropogenic"
510 contribution was only a small fraction of the total source, the uncertainty ranges of the source
511 signatures are larger. Therefore, the uncertainties for the early part were excluded when
512 calculating the 1σ uncertainties over the entire period from the generated scenarios. This
513 applies to all anthropogenic isotope signatures.

514 The budget calculations suggest an overall trend towards more enriched anthropogenic
515 emissions, but the uncertainties are large. Mathematically, this trend arises from the fact that
516 the isotope reconstructions yield relatively linear temporal isotope trends, whereas the source
517 strength increases in a strongly non-linear fashion (Fig. 4). In the beginning of the record a
518 small increase in the source strength needs to produce a certain absolute isotope shift, whereas
519 a smaller increase in the source strength is needed during later years to cause a similar isotope
520 shift. This can only be solved mathematically by a lower $\delta^{15}\text{N}^{\text{av}}$ value for the small
521 "anthropogenic" emissions in the early part of the firm record. A constant $\delta^{15}\text{N}^{\text{av}}$ source

522 signature would result in a small temporal change in $\delta^{15}\text{N}^{\text{av}}$ of atmospheric N_2O in the
523 beginning of the record and increasing isotope trends with increasing emissions, similar to the
524 exponential curves that were fitted to the firn air data in Röckmann et al. (2003).

525 The $\delta^{18}\text{O}$ of the total source varies within (27.2 ± 2.6) ‰ over the entire period. $\delta^{18}\text{O}$ does not
526 show significant decadal scale oscillations because the reconstructed scenario for $\delta^{18}\text{O}$ is even
527 more linear than the $\delta^{15}\text{N}^{\text{av}}$ scenario. For this reason, as explained above, in the best fit
528 scenario the $\delta^{18}\text{O}$ of the anthropogenic source for the initial 30 years has a more depleted
529 value starting with (7.7 ± 2.6) ‰ in year 1940, reaching (31.1 ± 2.6) ‰ in year 1975 and
530 remaining around this value until 2008 (Fig. 4). However, the relatively larger uncertainty
531 envelopes for the atmospheric history of $\delta^{18}\text{O}$ actually allow scenarios with smaller $\delta^{18}\text{O}$
532 changes in the beginning of the record and larger changes in the later period, which means
533 that the reconstruction does not exclude a constant value for the anthropogenic $\delta^{18}\text{O}$ source
534 signature. The available dataset thus does not allow quantifying a long-term trend in $\delta^{18}\text{O}$.

535 For the position dependent ^{15}N signatures of the total source no significant long-term trends
536 were detected. For $\delta^{15}\text{N}^{\alpha}$ no decadal scale variability is observed, whereas for $\delta^{15}\text{N}^{\beta}$ a
537 temporal variability is observed similar to the $\delta^{15}\text{N}^{\text{av}}$. The uncertainty ranges for $\delta^{15}\text{N}^{\alpha}$ and
538 $\delta^{15}\text{N}^{\beta}$ are about a factor 2 greater than for $\delta^{15}\text{N}^{\text{av}}$, which is due to the larger analytical error
539 that leads to higher uncertainties in the scenario reconstructions. $\delta^{15}\text{N}^{\alpha}$ varies in the range ($-$
540 3.0 ± 1.9) ‰, $\delta^{15}\text{N}^{\beta}$ in the range (-11.7 ± 2.3) ‰.

541 The temporal evolution of $\delta^{15}\text{N}^{\alpha}$ of the anthropogenic source looks similar to that of $\delta^{18}\text{O}$, but
542 with even larger variations and uncertainties with a total average of (-8.1 ± 1.7) ‰. $\delta^{15}\text{N}^{\alpha}$
543 increased from (-18.2 ± 1.7) ‰ in 1940 to an average of (-5.4 ± 1.7) ‰ in 1975 and retained
544 this value until 2008. In contrast, $\delta^{15}\text{N}^{\beta}$ is similar to that of $\delta^{15}\text{N}^{\text{av}}$ with a total anthropogenic
545 source average of (-26.1 ± 8.4) . $\delta^{15}\text{N}^{\beta}$ initially decreases from (-19.1 ± 8.4) ‰ to (-42.0 ± 8.4) ‰
546 in 1955 only to increase again to (-10.6 ± 8.4) ‰ in year 1990 and then decrease again to $(-$
547 $26.0\pm 8.4)$ ‰ in 2008.

548 **4 Discussion**

549 The N_2O mole fraction atmospheric history from our multi-site reconstruction is in agreement
550 with recent work from Meinshausen et al. (2016) who combined all available published N_2O
551 data (atmospheric, firn, ice) in order to reconstruct a historical atmospheric record of the past

552 2000 years. It differs slightly from the one determined by Battle et al. (1996) and to smaller
553 extent with Machida et al. (1995).

554 Battle et al. (1996) collected firn air data and Machida et al. (1995) used ice data. Both studies
555 used samples from a single Antarctic site. One could argue that the difference is due to an
556 interhemispheric difference, but it is too large to be explained by this alone. In the past, N₂O
557 mole fraction measurements have been reported on different calibration scales, which is likely
558 to explain part of the differences between individual studies. Furthermore, differences in the
559 firn air model and possible differences between sites may contribute. In our case we used
560 measurements from 5 sites to constrain our model while Battle et al. (1996) and Machida et
561 al. (1995) used only one site. In addition, the atmospheric histories of up to 9 known gases
562 (depending on site, Witrant et al. 2012) were used to constrain diffusivity in our model while
563 Battle et al. (1996) only used two gases."

564 From the combination of the firn air reconstruction with a simple two-box model we conclude
565 that N₂O emissions increased from (11.9±1.7) Tg a⁻¹ N in 1940 to (16.4±1.7) Tg a⁻¹ N in
566 2008. This agrees, within uncertainties, with previous firn reconstruction studies from
567 Ishijima et al. (2007) and Park et al. (2012) and bottom-up approaches using emission
568 databases (Syakila and Kroeze, 2013; Kroeze et al., 1999). A more recent study by Thompson
569 et al. (2014b) performed inversions of atmospheric measurements for 2006 to 2008 with
570 multiple models and reported emissions of 16.1-18.7 Tg a⁻¹ N for 2008, which is also in
571 agreement with our findings.

572 To investigate the effect the N₂O lifetime on the N₂O isotopic signatures (Prather et al. (2015)
573 we performed a sensitivity study where we linearly changed the N₂O lifetime from 123 years
574 pre-industrially (≈1750) to 119 years in modern times (2008). The results are shown in
575 Appendix D, where the effect on the emission strength and isotopic composition is discussed
576 in detail. Results from this sensitivity study showed that the effect of a decreasing lifetime
577 gives higher N₂O emissions for year 2008 while keeping the same pre-industrial value,
578 confirming the sensitivity to the lifetime in line with Prather et al. (2015). This change in
579 lifetime in the model leads to changes in the isotope signatures of the order of (2.0±1.0) ‰.
580 The lifetime effect is most pronounced for the earliest part of the record (<1970) where the
581 reconstruction uncertainties are larger than this systematic uncertainty.

582 We furthermore investigated the sensitivity to the value of F_{exch} (stratosphere – troposphere
583 flux) between a low and high value of 0.16 and 0.28 Tmol s⁻¹, respectively following

584 Appenzeller et al. (1996) and Holton et al. (1990) with the default value being 0.22 Tmol s^{-1} .
585 As shown in Appendix D, the isotope values are not very sensitive to the changes in F_{exch} , the
586 results are well within the uncertainty envelopes.

587 The increase in N_2O emissions over the past decades resulted in an overall decrease of all
588 isotopic signatures of atmospheric N_2O with time. The isotopic signature of the total source of
589 N_2O (Fig. 4, middle panels) is strongly depleted in all heavy isotopes compared to
590 tropospheric N_2O (Table 3), which is due to the strong enrichment associated with the
591 removal in the stratosphere. In Table 3 the isotopic composition for the pre-industrial period
592 (≈ 1750) ($\delta_{\text{nat,pi}}$) is compared with the derived anthropogenic source signature derived from
593 our multi-site reconstruction (δ_{anth} , averaged from 1940 to 2008). The results show that the
594 anthropogenic source is more depleted in heavy isotopes than the natural one for all
595 signatures, confirming results from studies prior to firm air measurements (Rahn and Wahlen,
596 2000), and from studies that used forward firm air modelling on measurements from individual
597 sites (Park et al., 2012; Ishijima et al., 2007; Röckmann et al., 2003). It is important to
598 remember that we assume the natural sources to be constant, but the method itself does not
599 provide evidence for this.

600 Anthropogenic N_2O emissions are dominated by agricultural soil (70 %) with smaller
601 contributions from automobiles, coal combustion, biomass burning and industry. Oceanic
602 emissions were previously assumed to be only natural. However, the latest IPCC Assessment
603 Report (Ciais et al., 2013) for the first time separated oceanic emissions into a natural and an
604 anthropogenic component, e.g. due to atmospheric N deposition to rivers (Syakila and
605 Kroeze, 2011; Duce et al., 2008; Kroeze et al., 2005). The oceanic fraction of the
606 anthropogenic source was estimated as $1 \text{ Tg a}^{-1} \text{ N}$.

607 N_2O emitted from agricultural soils and biomass burning is more depleted in $\delta^{15}\text{N}^{\text{av}}$ and $\delta^{18}\text{O}$
608 than the tropospheric background (Park et al., 2011; Goldberg et al., 2010; Ostrom et al.,
609 2010; Tilsner et al., 2003; Perez et al., 2001; 2000) while N_2O emitted from other minor
610 sources, such as automobiles, coal combustion and industry, has values closer to tropospheric
611 N_2O values (Syakila and Kroeze, 2011; Toyoda et al., 2008; Ogawa and Yoshida, 2005a;
612 2005b). An increase of strongly depleted agricultural emissions in the first part of our
613 reconstruction, followed by a decreasing relative contribution from agriculture and increasing
614 contributions from more enriched sources like industry, automobiles and coal combustion,
615 could qualitatively explain the reconstructed changes of isotope signatures of both the total

616 source and the anthropogenic component. The global N₂O budget study from Syakila and
617 Kroeze (2011) indicates that agricultural emissions were 78 % of the total during the 1940-
618 1980 period with little input from industry, vehicle exhaust and coal combustion. After 1980
619 the relative share of agricultural emissions dropped to 64 %, while the other sources
620 increased, supporting our suggestion.

621 According to FAO statistics (<http://www.fao.org/faostat/en/#data/GY/visualize>), emissions
622 from synthetic nitrogenous fertilizers increased between 1961 and 1985, then stayed relatively
623 constant or even decreased until 2000, and increased again after 2000. The reasons of the
624 decrease between 1985 and 2000 are a shift towards organic soil cultivation in combination
625 with more efficient agricultural methods and fertilizer use. This variation in fertilizer use
626 qualitatively matches with the temporal evolutions of our reconstructed source signatures, but
627 the trends in the reconstructions are likely too large to be explained by this source change
628 only.

629 Although the decadal variability for $\delta^{15}\text{N}^{\text{rav}}$ and $\delta^{15}\text{N}^{\beta}$ appears statistically significant with
630 respect to the choice of scenarios constructed within the error bars of the firm air
631 reconstruction, additional systematic uncertainties in this reconstruction could potentially
632 produce such trends artificially from small undulations on the scenarios, since the emissions
633 are related to the derivative of the trend. As it is possible to draw straight lines within
634 uncertainty envelopes of the scenarios, the decadal variability may not be robust. An increase
635 of the regularization term by 10 confirms that the generated scenarios are straight lines well
636 within the uncertainty envelopes, thus the decadal variability could be an artifact of the model
637 (see Appendix C).

638 Additional evidence for potential changes in the N₂O source composition between the pre-
639 industrial and present atmosphere may be derived from the position-dependent ¹⁵N signatures,
640 quantified by the ¹⁵N site preference. Table 3 shows that the difference in the $\delta^{15}\text{N}^{\text{rav}}$ signature
641 between the pre-industrial and the anthropogenic source derived from our reconstruction is
642 primarily due to a change at position $\delta^{15}\text{N}^{\beta}$, whereas $\delta^{15}\text{N}^{\alpha}$ remains relatively constant. This is
643 reflected by a larger difference in $\delta^{15}\text{N}^{\text{sp}}$ between natural and anthropogenic emissions, which
644 could indicate a temporal change in production processes.

645 Sutka et al. (2006) suggested that there may be two distinct classes of N₂O sources with
646 different $\delta^{15}\text{N}^{\text{sp}}$. N₂O produced during nitrification and fungal denitrification had a high $\delta^{15}\text{N}^{\text{sp}}$
647 of (33±5) ‰ and N₂O from denitrification and nitrifier denitrification had a low $\delta^{15}\text{N}^{\text{sp}}$ of

648 (0±5) ‰. Park et al., (2012) used these two endmembers to calculate a change in the relative
 649 fractions of these source classes over time based on their firm air data. Although this approach
 650 is strongly simplified and several other sources and factors may contribute (Toyoda et al.,
 651 2015), we use the results from our box model calculations (Table 3) in a similar way to
 652 estimate the fraction of the two source categories according to the following simple mass
 653 balance calculation:

$$654 \quad F_{\text{high}} = \frac{\delta^{15} \text{N}_{\text{meas}}^{\text{sp}} - \delta^{15} \text{N}_{\text{low}}^{\text{sp}}}{\delta^{15} \text{N}_{\text{high}}^{\text{sp}} - \delta^{15} \text{N}_{\text{low}}^{\text{sp}}} \quad (11)$$

655 This returns a fractional contribution of the $\delta^{15} \text{N}_{\text{high}}^{\text{sp}}$ component of (19±4) % to the total pre-
 656 industrial emissions and (35±11) % to the total present source. The errors were derived by
 657 propagating the errors of the $\delta^{15} \text{N}^{\text{sp}}$ endmembers and $\delta^{15} \text{N}_{\text{meas}}^{\text{sp}}$ within the ranges stated above.
 658 We note that the errors associated with the precise isotopic composition of the endmembers
 659 are correlated if the values of $\delta^{15} \text{N}^{\text{sp}}$ for the two endmembers remain relatively constant in
 660 time. Therefore, the change in the relative fraction of the two categories is likely better
 661 constrained than the absolute values.

662 Splitting the total present emission strength into a natural (pre-industrial, 11.0 Tg a⁻¹ N) and
 663 anthropogenic (5.4 Tg a⁻¹ N) component, we derive a fraction of the $\delta^{15} \text{N}_{\text{high}}^{\text{sp}}$ component
 664 (which includes nitrification) of (54±26) % for the "anthropogenic" emissions. This is another
 665 piece of evidence for agricultural sources being the main contributor to the N₂O increase,
 666 because nitrification-dominated agricultural emissions can be associated with the $\delta^{15} \text{N}_{\text{high}}^{\text{sp}}$
 667 component.

668 The temporal changes of the derived fraction of nitrification are in good qualitative agreement
 669 with the results from Park et al. (2012), who reported a change of (13±5) % from 1750 to
 670 (23±13) % today. However, the absolute numbers derived from our study are higher than the
 671 results from Park et al. (2012). The difference is due to the fact that different apparent isotope
 672 fractionations during stratospheric removal (ϵ_{app}) are used in the mass balance model (Table
 673 3; eq. 7,8). In our study we used the averaged lowermost stratospheric apparent isotope
 674 fractionations from Kaiser et al. (2006), which we consider more representative than the
 675 numbers used by Park et al. (2012). Using different values for ϵ_{app} causes a shift in the
 676 isotopic source signatures from the mass balance model. The choice of this value thus adds a

677 systematic source of uncertainty to the absolute value of the $\delta^{15}\text{N}_{\text{high}}^{\text{SP}}$ fractions reported above
678 (F_{high}).

679 Nevertheless, this systematic uncertainty should not alter the overall *change* in F_{high} from pre-
680 industrial to modern times and the results from our multi-site reconstruction of the isotopic
681 composition of N_2O thus confirm the suggestion by Park et al. (2012) that the relative
682 importance of the high-SP component (presumably nitrification) has increased with increasing
683 mole fraction since pre-industrial times.

684 **5 Conclusions**

685 The temporal evolution of the total N_2O emission fluxes and the source isotopic composition
686 have been estimated in a top-down approach using a multi-site reconstruction of N_2O mole
687 fraction and isotopic composition from 6 firm air samplings at 5 different Arctic and Antarctic
688 locations in a two-box model. The results from a mass balance model constrain the source
689 strength and suggest a total increase in N_2O emissions of $(4.5 \pm 1.7) \text{ Tg a}^{-1} \text{ N}$ between the 1940
690 and 2008 due to anthropogenic processes. This agrees with previous top-down estimates, but
691 deviates from bottom-up model estimates, which suggest higher N_2O emission increases. A
692 significant source of the uncertainty in top-down estimates is a possible change in the N_2O
693 lifetime over the reconstruction period, which we have quantified following the recent results
694 from Prather et al. (2015).

695 The reconstruction of mole fraction and isotopic composition was used to investigate
696 temporal changes in the isotopic signature of N_2O emissions over the study period. The
697 average total source for $\delta^{15}\text{N}^{\text{av}}$ and $\delta^{15}\text{N}^{\beta}$ shows no statistically significant long-term trend but
698 possibly significant decadal scale variability. For $\delta^{18}\text{O}$ and $\delta^{15}\text{N}^{\alpha}$ of the total N_2O source, no
699 significant temporal changes can be detected with the present dataset because the
700 uncertainties are large, especially in the beginning of the reconstruction period.

701 When the total source is split into a constant natural and a varying anthropogenic component,
702 the reconstruction of the δ values of the anthropogenic source indicates a significant increase
703 of $\delta^{15}\text{N}^{\text{av}}$ from the early to the modern part of the record. This originates from the near-linear
704 isotope histories of the best guess scenario, which would imply that small emissions in the
705 early part had a similar absolute effect on the δ values as stronger emissions in the latter part.
706 A similar effect for $\delta^{18}\text{O}$ is likely, but not significant given the larger uncertainties for this
707 signature.

708 Nevertheless, the isotope signal in $\delta^{15}\text{N}^{\text{av}}$ may also be a signal for changing source
709 contributions over time. Bottom-up models suggest that N_2O emitted from agricultural soils
710 was the dominant contributor to the anthropogenic N_2O increase in the first decades. Smaller
711 contributions due to emissions from more enriched sources, like industry, automobiles and
712 coal combustion increased. This may have contributed to an isotope enrichment of the
713 emissions, which is not detectable within the error bars for the other isotope signatures.
714 However, one has to be cautious with a firm interpretation of these trends since the
715 reconstruction method itself may also induce decadal variability if the smoothness of the
716 scenario is incorrectly constrained.

717 Results from the mass balance model yield an increase in ^{15}N site preference between the pre-
718 industrial and modern total N_2O source. When this trend is evaluated with a simplified two-
719 endmember mixing model, the results suggest an increase of nitrification sources relative to
720 denitrification-related sources over the industrial period.

721 **Acknowledgements**

722 We thank the teams involved in the firm air sampling at NEEM site during the 2008 and 2009
723 field seasons. NEEM is directed and organized by the Centre of Ice and Climate at the Niels
724 Bohr Institute, University of Copenhagen, Denmark and the US National Science Foundation,
725 Office of Polar Programs. It is supported by funding agencies and institutions in Belgium
726 (FNRS-CFB and FWO), Canada (NRCan/GSC), China (CAS), Denmark (FIST), France
727 (IPEV, CNRS/INSU, CEA and ANR), Germany (AWI), Iceland (RannIs), Japan (NIPR),
728 Korera (KOPRI), The Netherlands (NWO/ALW and NWO/NPP), the United Kingdom
729 (NERC NE/F021194/1) and the USA (US NSF, Office of Polar Programs). This project was
730 financially supported by the Dutch Science Foundation (NWO), projects 851.30.020 &
731 865.07.001.

732 **References**

- 733 Allin, S. J., Laube, J. C., Witrant, E., Kaiser, J., McKenna, E., Dennis, P., Mulvaney, R.,
734 Capron, E., Martinerie, P., Röckmann, T., Blunier, T., Schwander, J., Fraser, P. J.,
735 Langenferls, R. L., and Sturges, W. T.: Chlorine isotope composition in chlorofluorocarbons
736 CFC-11, CFC-12 and CFC-113 in firn, stratospheric and tropospheric air, *Atmos. Chem.*
737 *Phys.*, 15, 6867-6877, doi:10.5194/acp-15-6867-2015, 2015.
- 738 Battle, M., Bender, M., Sowers, T., Tans, P. P., Butler, J. H., Elkins, J. W., Ellis, J. T.,
739 Conway, T., Zhang, N., Lang, P., and Clarke, A. D.: Atmospheric gas concentrations over the
740 past century measured in air from firn at South Pole, *Nature*, 383, 231-235, 1996.
- 741 Bernard, S., Röckmann, T., Kaiser, J., Barnola, J.-M., Fischer, H., Blunier, T., and
742 Chappellaz, J.: Constraints on N₂O budget changes since pre-industrial time from new firn air
743 and ice core isotope measurements, *Atmos. Chem. Phys.*, 6, 493–503, doi:10.5194/acp-6-493-
744 2006, 2006.
- 745 Buizert, C., Sowers, T., and Blunier, T.: Assessment of diffusive isotopic fractionation in
746 polar firn, and application to ice core trace gas records, *Earth Planet. Sci. Lett.*, 361, 110–119,
747 2013.
- 748 Butterbach-Bahl, K., and Dannenmann, M.: Denitrification and associated soil N₂O emissions
749 due to agricultural activities in a changing climate, *Curr. Op. Environ. Sus.*, 3(5), 389–395,
750 doi:10.1016/j.cosust.2011.08.004, 2011.
- 751 Ciais, P., Sabine, C., Bala, G., Bopp, L., Brovkin, V., Canadell, J., Chhabra, A., DeFries, R.,
752 Galloway, J., Heimann, M., Jones, C., Le Quéré, C., Myneni, R.B., Piao, S., and Thornton, P.:
753 Carbon and other biogeochemical cycles. *Climate Change 2013: The Physical Science Basis,*
754 *Contribution of Working Group I to the Fifth Assessment Report of the Intergovernmental*
755 *Panel on Climate Change*, Cambridge University Press, Cambridge, United Kingdom and
756 New York, NY, USA, 2013.
- 757 Crutzen, P. J., Mosier, A. R., Smith, K. A., and Winiwarter, W.: N₂O release from agro-
758 biofuel production negates global warming reduction by replacing fossil fuels, *Atmos. Chem.*
759 *Phys.*, 8, 389-395, doi:10.5194/acp-8-389-2008, 2008.

760 Crutzen, P.J.: The role of NO and NO₂ in the chemistry of the troposphere and stratosphere,
761 *Annual review of earth and planetary sciences*, 7, 443-472, 1979.

762 Davidson, E. A.: The contribution of manure and fertilizer nitrogen to atmospheric nitrous
763 oxide since 1860, *Nat. Geosci.*, 2(9), 659–662, doi:10.1038/ngeo608, 2009.

764 Duce, R. A., LaRoche, J., Altieri, K., Arrigo, K. R., Baker, A. R., Capone, D. G., Cornell, S.,
765 Dentener, F., Galloway, J., and Ganeshram, R. S.: Impacts of atmospheric anthropogenic
766 nitrogen on the open ocean, *Science*, 320, 893-897, 2008.

767 Freing, A., Wallace, D. W. R., and Bange, H. W.: Global oceanic production of nitrous oxide,
768 *Phil. Trans. R. Soc. Lond., Series B*, 367(1593), 1245–55, doi:10.1098/rstb.2011.0360, 2012.

769 Hirsch, A., Michalak, A., Bruhwiler, L., Peters, W., Dlugokencky, E., and Tans, P.: Inverse
770 modelling estimates of the global nitrous oxide surface flux from 1998-2001, *Gl. Biochem.*
771 *Cycl.*, 20, GB 1008, doi: 10.1029/2004GB002443, 2006.

772 Holton, J. R.: On the global exchange of mass between stratosphere and troposphere, *J.*
773 *Atmos. Sci.* , 47(3), 392-395, 1990.

774 Houghton, J. T., Meira Filho, L. G., Bruce, J., Lee, H., Callander, B. A, Haites, E., Harris, N.,
775 and Maskell, K.: *Climate Change 1994: Radiative Forcing of Climate Change and an*
776 *Evaluation of the IPCC IS 92 Emission Scenarios*, Cambridge University Press, Cambridge,
777 UK, 1994.

778 Ishijima, K., Sugawara, S., Kawamura, K., Hashida, G., Morimoto, S., Murayama, S., Aoki,
779 S.: Temporal variations of the atmospheric nitrous oxide concentration and its $\delta^{15}\text{N}$ and $\delta^{18}\text{O}$
780 for the latter half of the 20th century reconstructed from firn air analyses, *J. Geophys. Res.*,
781 112(D3), doi:10.1029/2006JD007208, 2007.

782 Kaiser, J., Brenninkmeijer, C.A.M., Röckmann, T.: Intramolecular ^{15}N and ^{18}O fractionation
783 in the reaction of N₂O with O(¹D) and its implications for the stratospheric N₂O isotopic
784 signature, *J. Geophys. Res.*, 107 (4214), doi:10.1029/2001JD001506, 2002.

785 Kaiser, J., Röckmann T., and Brenninkmeijer, C.A.M.: Complete and accurate mass
786 spectrometric isotope analysis of tropospheric nitrous oxide, *J. Geophys. Res.*, 108(D15), 1–
787 17, doi:10.1029/2003JD003613, 2003.

788 Kaiser, J., Engel, A., Borchers, R., and Röckmann, T.: Probing stratospheric transport and
789 chemistry with new balloon and aircraft observations of the meridional and vertical N₂O
790 isotope distribution, *Atmos. Chem. Phys.*, 6, 3535-3556, doi:10.5194/acp-6-3535-2006, 2006.

791 Kaiser, J., and Röckmann T.: Correction of mass spectrometric isotope ratio measurements
792 for isobaric isotopologues of O₂, CO, CO₂, N₂O and SO₂, *Rap. Commun. Mass Spec.*, 3997–
793 4008, doi: 10.1002/rcm.3812, 2008.

794 Kim, K. R., and Craig, H.: Nitrogen-15 and Oxygen-18 Characteristics of Nitrous Oxide: A
795 global perspective, *Science*, 262, 1855-1857, 1993.

796 Kim, K. R., Craig, H.: Two-isotope characterization of N₂O in the Pacific Ocean and
797 constraints on its origin in deep water, *Nature*, 347, 58-61, doi:10.1038/347058a0, 1990.

798 Kool, D. M., Wrage, N., Oenema, O., Harris, D., and Groenigen, J. W. Van.: The ¹⁸O
799 signature of biogenic nitrous oxide is determined by O exchange with water, *Rap. Commun.*
800 *Mass Spec.*, 104–108, doi:10.1002/rcm.3859, 2009.

801 Kroeze, C., Mosier, A., and Bouwman, L.: Closing the global N₂O budget: a retrospective
802 analysis 1500-1994, *Glob. Biogeochem. Cycl.*, 13, 1-8, doi: 10.1029/1998GB900020, 1999.

803 Kroeze, C., Dumont, E., and Seitzinger, S. P.: New estimates of global emissions of N₂O from
804 rivers and estuaries, *Environ. Science*, 2, 159-165, doi:10.1080/15693430500384671, 2005.

805 Löscher, C.R., Kock, A., Könneke, M., LaRoche, J., Bange, H. W., and Schmitz, R. A.:
806 Production of oceanic nitrous oxide by ammonia-oxidizing archaea, *Biogeosciences*, 9, 2419-
807 2429, doi:10.5194/bg-9-2419-2012, 2012.

808 MacFarling Meure, C., Etheridge, D., Trudinger, C., Steele, P., Langenfelds, R., van Ommen,
809 T., Smith, A., and Elkins, J.: Law Dome CO₂, CH₄ and N₂O ice core records extended 2000
810 years BP, *Geophys. Res. Letters*, 33, 2000-2003, doi:10.1029/2006GL026152, 2006.

811 Machida, T., Nakazawa, T., Fujii, Y., Aoki, S., and Watanabe, O.: Increase in the atmospheric
812 nitrous oxide concentration during the last 250 years, *Geophys. Res. Letters*, 22, 2921-2924,
813 1995.

814 Maeda, K., Toyoda, S., Shimojima, R., Osada, T., Hanajima, D., Morioka, R., and Yoshida,
815 N.: Source of nitrous oxide emissions during the cow manure composting process as revealed
816 by isotopomer analysis of and amoA abundance in betaproteobacterial ammonia-oxidizing
817 bacteria, *Appl. Environ. Microbiol.*, 76(5), 1555–62, doi:10.1128/AEM.01394-09, 2010.

818 Martinerie, P., Nourtier-Mazauric, E., Barnola, J.-M., Sturges, W. T., Worton, D. R., Atlas,
819 E., Brasseur, G. P.: Long-lived halocarbon trends and budgets from atmospheric chemistry
820 modelling constrained with measurements in polar firm, *Atmos. Chem. Phys*, 9, 3911-3934,
821 doi:10.5194/acp-9-3911-2009, 2009.

822 McElroy, M. B., and McConnell, J. C.: Nitrous oxide: A natural source of stratospheric NO,
823 *Journal of Atmospheric Sciences*, 28, 1095-1098, 1971.

824 McLinden, C. A., Prather, M. J., Johnson M. S.: Global modeling of the isotopic analogues of
825 N₂O: Stratospheric distributions, budgets and the ¹⁷O-¹⁸O mass-independent anomaly, *J.*
826 *Geophys. Res.*, 108(D8), doi:10.1029/2002JD002560, 2003.

827 Meinshausen, M., Vogel, E., Nauels, A., Lorbacher, K., Meinshausen, N., Etheridge, D.,
828 Frazer, P., Montzka, S. A., Rayner, P., Trudinger, C., Krummel, P., Beyerle, U., Cannadell, J.
829 G., Daniel, J. S., Enting, I., Law, R. M., O'Doherty, S., Prinn, R. G., Reimann, S., Rubino,
830 M., Velders, G. J. M., Vollmer, M. K., and Weiss, R.: Historical greenhouse gas
831 concentrations, *Geosci. Model Dev. Discuss*, doi:10.5194/gmd-2016-169, in review, 2016.

832 Minschwaner, K., Salawitch, R.J., McElroy, M.B.: Absorption of Solar Radiation by O₂:
833 Implications for O₃ and lifetimes of N₂O, CFCl₃, and CF₂Cl₂, *J. Geophys. Res.*, 98, 10543-
834 10561, doi: 10.1029/93JD00223, 1993.

835 Ogawa, M., and Yoshida, N.: Intramolecular distribution of stable nitrogen and oxygen
836 isotopes of nitrous oxide emitted during coal combustion, *Chemosphere*, 61, 877-887, 2005a.

837 Ogawa, M., and Yoshida, N.: Nitrous oxide emission from the burning of agricultural residue.
838 *Atmos. Environ.*, 39, 3421-3429, 2005b.

839 Ostrom, N. E., and Ostrom, P. H.: The isotopomers of Nitrous Oxide: Analytical
840 considerations and application to resolution of microbial production pathways, Baskaran, M.,
841 Handbook of Environmental Isotope Geochemistry, Advances in Isotope Geochemistry,
842 Springer, Verlag, Berlin, Heidelberg, 453-476, 2011.

843 Park, S., Atlas, E. L., and Boering, K. A.: Measurements of N₂O isotopologues in the
844 stratosphere: Influence of transport on the apparent enrichment factors and the isotopologue
845 fluxed to the troposphere, *J. Geophys. Res.*, 109, doi:10.1029/2003JD003731, 2004.

846 Park, S., Croteau, P., Boering, K. A., Etheridge, D. M., Ferretti, D., Fraser, P. J., and
847 Trudinger, C. M.: Trends and seasonal cycles in the isotopic composition of nitrous oxide
848 since 1940, *Nat. Geosci.*, 5(4), 261–265, doi:10.1038/ngeo1421, 2012.

849 Pérez, T., Trumbore, S. E., Tyler, S. C., Davidson, E. A., Keller, M., and Camargo, P. de.:
850 Isotopic variability of N₂O emissions from tropical forest soils, *Glob. Biogeochem. Cycl.*,
851 14(2), 525-535, 2000.

852 Pérez, T., Trumbore, S. E., Tyler, S. C., Matson, P. A., Ortiz-Monasterio, I., Rahn, T., and
853 Griffith, D. W. T.: Identifying the agricultural imprint on the global N₂O budget using stable
854 isotopes, *J. Geophys. Res.*, 106(D9), 9869-9878, 2001.

855 Popp, B. N., Westley, M. B., Toyoda, S., Miwa, T., Dore, J. E., Yoshida, N., Rust, T. M.,
856 Sansone, F. J., Russ, M. E., Ostrom, N. E., and Ostrom, P. H.: Nitrogen and oxygen
857 isotopomeric constraints on the origins and sea-to-air flux of N₂O in the oligotrophic
858 subtropical North Pacific gyre, *Glob. Biogeochem. Cycl.*, 16, 1064,
859 doi:10.1029/2001GB001806, 2002.

860 Potter, K. E.: Nitrous oxide (N₂O) isotopic composition in the troposphere: instrumentation,
861 observations at Mace Head, Ireland, and regional modeling, PhD thesis, Department of Earth,
862 Atmospheric, and Planetary Sciences at the Massachusetts Institute of Technology, 2011.

863 Prather, M. J., et al.: Measuring and modeling the lifetime of nitrous oxide including its
864 variability, *J. Geophys. Res. Atmos.*, 120, 5693-5705, doi: 10.1002/2015JD023267, 2015.

865 Rahn, T., and Wahlen, M.: Stable isotope enrichment in stratospheric nitrous oxide, *Science*,
866 278, 1776-1778, doi: 10.1126/science.278.5344.1776, 1997.

867 Rahn, T., Zhang, H., Wahlen, M., and Blake, G. A.: Stable isotope fractionation during
868 ultraviolet photolysis of N₂O, *Geophys. Res. Lett.*, 25, 4489-4492, 1998.

869 Rahn, T., and Wahlen, M.: A reassessment of the global isotopic budget of atmospheric
870 nitrous oxide, *Glob. Biogeochem. Cycl.*, 14, 537-543, 2000.

871 Ravishankara, A. R., Daniel, J. S., and Portmann, R. W.: Nitrous oxide (N₂O): the dominant
872 ozone-depleting substance emitted in the 21st century, *Science*, 326(5949), 123–125,
873 doi:10.1126/science.1176985, 2009.

874 Röckmann, T., Kaiser, J., Brenninkmeijer, C. A. M., Crowley, J. N., Borchers, R., Brand, W.
875 A., and Crutzen, J.: Isotopic enrichment of nitrous oxide (¹⁵N¹⁴NO, ¹⁴N¹⁵NO, ¹⁴N¹⁴N¹⁸O) in
876 the stratosphere and in the laboratory, *J. Geophys. Res.*, 106(D10), 10403-10410,
877 doi:10.1029/2000JD900822, 2001.

878 Röckmann, T., Kaiser, J., Brenninkmeijer, C. A. M., and Brand, W. A.: Gas
879 chromatography/isotope-ratio mass spectrometry method for high-precision position-
880 dependent ¹⁵N and ¹⁸O measurements of atmospheric nitrous oxide, *Rap. Commun. Mass*
881 *Spectrom.*, 17(16), 1897–1908, doi:10.1002/rcm.1132, 2003.

882 Röckmann, T., Kaiser, J., Brenninkmeijer, C. A. M.: The isotopic fingerprint of the pre-
883 industrial and the anthropogenic N₂O source, *Atmos. Chem. Phys.*, 3, 315-323,
884 doi:10.5194/acp-3-315-2003, 2003.

885 Röckmann, T., and Levin, I.: High-precision determination of the changing isotopic
886 composition of atmospheric N₂O from 1990 to 2002, *J. Geophys. Res.*, 110(D21), 1–8,
887 doi:10.1029/2005JD006066, 2005.

888 Santoro, A. E., Buchwald, C., Mellvin, M. R., and Casciotti, K. L.: Isotopic signature of N₂O
889 produced by marine ammonia-oxidizing archaea, *Science*, 333(6047), 1282–1285,
890 doi:10.1126/science.1208239, 2011.

891 Sapart, C. J., van der Veen, C., Vigano, I., Brass, M., van de Wal, R. S. W., Bock, M.,
892 Fischer, H., Sowers, T., Buizert, C., Sperlich, P., Blunier, T., Behrens, M., Schmitt, J., Seth,
893 B., and Röckmann, T.: Simultaneous stable isotope analysis of methane and nitrous oxide of
894 ice core samples, *Atmos. Meas. Tech.*, 4, 2607–2618, doi:10.5194/amt-4-2607-2011, 2011.

895 Sapart, C. J., Martinerie, P., Witrant, E., Chappellaz, J., van de Wal, R. S. W., Sperlich, P.,
896 van der Veen, C., Bernard, S., Sturges, W. T., Blunier, T., Schwander, J., Etheridge, D.,
897 Röckmann, T.: Can the carbon isotopic composition of methane be reconstructed from multi-
898 site firn air measurements?, *Atmos. Chem. Phys.*, 13, 6993-7005, doi:10.5194/acp-13-6993-
899 2013, 2013.

900 Stocker, T. F., Qin, D., Plattner, G.-K., Tingor, M., Allen, S. K., Boschung, J., Nauels, A.,
901 Xia, Y., Bex, V., Midgley, P. M. et al.: IPCC, 2013: Climate Change 2013: The physical
902 Science Basis. Contribution of Working Group I to the Fifth Assessment Report of the
903 Intergovernmental Panel on Climate Change, Cambridge University Press, Cambridge, United
904 Kingdom and New York, NY, USA, 2013.

905 Sowers, T., Rodebaugh, A., Yoshida, N., and Toyoda, S.: Extending records of the isotopic
906 composition of atmospheric N₂O back to 1800 A.D. from air trapped in snow at the South
907 Pole and the Greenland Ice Sheet Project II ice core, *Global Biogeochemical Cycles*, 16(4),
908 1–10, doi: 10.1029/2002GB001911, 2002.

909 SPARC, 2013: SPARC Report on the Lifetimes of Stratospheric Ozone-Depleting
910 Substances, Their Replacements, and Related Species, edited by: Ko, M., Newman, P.,
911 Reimann, S., and Strahan, S, SPARC Report No. 6, WCRP-15, Zurich, Switzerland, 2013.

912 Suntharalingam, P., Buitenhuis, E., Le Quéré, C., Dentener, F., Nevison, C., Butler, J. H., and
913 Forster, G.: Quantifying the impact of anthropogenic nitrogen deposition on oceanic nitrous
914 oxide, *Geophysical Research Letters*, 39, doi:10.1029/2011GL050778, 2012.

915 Sutka, R. L., Ostrom, N. E., Ostrom, P. H., Breznak, J. A., Gandhi, H., Pitt, A. J., and Li, F.:
916 Distinguishing Nitrous Oxide Production from Nitrification and Denitrification on the Basis
917 of Isotopomer Abundances, *Appl. Environ. Microbiol.*, 72(1), 638–644,
918 doi:10.1128/AEM.72.1.638-644.2006, 2006.

919 Syakila, A., Kroeze, C., and Slomp, C. P.: Neglecting sinks for N₂O at the earth's surface:
920 does it matter?, *Journal of Integrative Environmental Sciences*, 7, 79-87,
921 doi:10.1080/1943815X.2010.497492, 2010.

922 Syakila, A., and Kroeze, C.: The global nitrous oxide budget revisited, *Greenhouse Gas*
923 *Measurement and Management*, 1(1), 17–26, doi:10.3763/ghgmm.2010.0007, 2011.

924 Thompson, R. L., Ishijima, K., Saikawa, E., Corazza, M., Karstens, U., Patra, P. K.,
925 Bousquet, P. (2014). TransCom N₂O model inter-comparison, Part II: Atmospheric inversion
926 estimates of N₂O emissions. *Atmospheric Chemistry and Physics Discussions*, 14(4), 5271–
927 5321.

928 Thompson, R. L., Patra, P. K., Ishijima, K., Saikawa, E., Corazza, M., Karstens, U.,
929 Bousquet, P.: TransCom N₂O model inter-comparison – Part 1: Assessing the influence of
930 transport and surface fluxes on tropospheric N₂O variability, *Atmos. Chem. Phys.* 14, 4349–
931 4368, doi:10.5194/acp-14-4349-2014, 2014.

932 Toyoda, S., Yamamoto, S., Arai, S., Nara, H., Yoshida, N., Kashiwajura, K., and Akiyama,
933 K.: Isotopomeric characterization of N₂O produced, consumed and, emitted by automobiles.,
934 *Rap. Comm. in Mass Spec.*, 22, 603-612, doi:10.1002/rcm.3400, 2008.

935 Wang, Z., Chappellaz, J., Martinerie, P., Park, K., Petrenko, V., Witrant, E., Emmons, L. K.,
936 Blunier, T., Brenninkmeijer, C. A. M., and Mak, J. E.: The isotopic record of Northern
937 Hemisphere atmospheric carbon monoxide since 1950: implications for the CO budget,
938 *Atmos. Chem. Phys.*, 12, 4365-4377, doi:10.5194/acp-12-4365-2012, 2012.

939 Westley, M. B., Popp, B. N., and Rust, T. M.: The calibration of the intramolecular isotope
940 distribution in nitrous oxide measured by isotope ratio mass spectrometry, *Rap. Comm. in*
941 *Mass. Spec.*, 21(3), 391-405, doi:10.1002/rcm.2828, 2007.

942 Witrant, E., Martinerie, P., Hogan, C., Laube, J.C, Kawamura, K., Capron, E., Montzka, S.
943 A., Dlugokencky, E. J., Etheridge, D., Blunier, T., and Sturges, W. T.: A new multi-gas
944 constrained model of trace gas non-homogeneous transport in firm: evaluation and behavior at
945 eleven polar sites, *Atmos. Chem. Phys.*, 12, 11465-11483, doi:10.5194/acp-12-11465-2012,
946 2012.

947 Witrant, E., Martinerie, P.: Input estimation from sparse measurements in LPV systems and
948 isotopic ratios in polar firm, IFAC Joint conferenc SSSC - 5th Symposium on System
949 Structure and Control, Grenoble, France, 150, 2013.

950 Yoshida, N., and Toyoda, S.: Constraining the atmospheric N₂O budget from intramolecular
951 site preference in N₂O isotopomers, *Nature*, 405, 330–334, doi:10.1038/35012558, 2000.

952

953 Table 1. Site information on the drilling locations of the North Greenland Ice core Project
 954 (NGRIP-01^{Ishijima}, NGRIP-01^{Bernard}), Berkner Island (BKN-03), North Greenland Eemian Ice
 955 drilling Project (NEEM-EU-08, NEEM-09), Dome Concordia (DC-99) and Dronning Maud
 956 Land (DML-98), where firn air samples were collected, and two key meteorological variables
 957 of each site.

Site	Location	Mean annual temperature (°C)	Surface accumulation rate (water equivalent) (cm a ⁻¹)	Sampling year
NGRIP-01 ¹	75° N 42° W	-31	20	2001
BKN-03 ²	79° S 45° W	-26	13	2003
NEEM-EU-08	77.4° N 51.1° W	-29	22	2008
NEEM-09	77.4° N 51.1° W	-29	22	2009
DC-99 ³	75° S 123° E	-53	3	1999
DML-98 ³	75° S 65° E	-38	6	1998

958 ¹ Data retrieved from Bernard et al. (2006), Ishijima et al. (2007)

959 ² Data retrieved from Bernard et al. (2006)

960 ³ Data retrieved from Röckmann et al. (2003)

961

962

963

964

965

966

967

968

969

970

971 Table 2. Detailed information in the mole fraction and the isotopic composition of the
 972 laboratory reference gases used for correcting each set of firn air samples.

Site	Sampling year	Mole fraction (nmol mol ⁻¹)	$\delta^{15}\text{N}^{\text{av}}$ (‰)	$\delta^{18}\text{O}$ (‰)	$\delta^{15}\text{N}^{\beta}$ (‰)	$\delta^{15}\text{N}^{\alpha}$ (‰)
NGRIP-01	2001	318	6.64	44.61	-2.79	16.07
BKN-03	2003	318	6.64	44.61	-2.79	16.07
NEEM- EU-08	2008	324	6.22	44.40	-3.08	15.52
NEEM-09	2009	318	6.38	44.92	-2.66	15.41
DC-99	1999	318	6.64	44.61	-2.79	16.07
DML-98	1998	318	6.64	44.61	-2.79	16.07

973
 974
 975
 976
 977
 978
 979
 980
 981
 982
 983
 984
 985
 986
 987
 988

989 Table 3. Emission fluxes and isotopic composition of the natural and anthropogenic source
 990 results from the mass balance model. Stratospheric isotope fractionation (ϵ_L) used in the mass
 991 balance model, and the respective results from Park et al. (2012).

Natural source (E_{nat}, $\delta_{nat,pi}$)¹		
	This study	Park et al. (2012)
E_{nat} (Tg a ⁻¹ N)	11.0±1.7	11.1
$\delta^{15}N^{av}$ (‰)	-5.2±0.2	-5.3±0.2
$\delta^{18}O$ (‰)	33.1±0.2	32.0±0.2
$\delta^{15}N^a$ (‰)	-1.9±1.0	-3.3±1.0
$\delta^{15}N^b$ (‰)	-8.3±1.1	-7.5±1.1
$\delta^{15}N^{sp}$ (‰)	6.4±1.5	4.2±1.5
Anthropogenic source (E_{anth}, δ_{anth})		
	This study	Park et al. (2012)
E_{anth} (Tg a ⁻¹ N)	5.4±1.7	6.6
$\delta^{15}N^{av}$ (‰)	-18.2±2.6	-15.6±1.2
$\delta^{18}O$ (‰)	27.2±2.6	32.0±1.3
$\delta^{15}N^a$ (‰)	-8.1±1.7	-7.6±6.2
$\delta^{15}N^b$ (‰)	-26.1±8.4	-20.5±7.1
$\delta^{15}N^{sp}$ (‰)	18.0±8.6	13.1±9.4
Stratospheric Loss¹		
	This study	Park et al. (2012)
F_{exch} (Tmol s ⁻¹)	0.22	NA
L (Tg a ⁻¹ N)	12.3	NA
$\epsilon_{app}^{15}N^{av}$ (‰)	-16.2	-14.9
$\epsilon_{app}^{18}O$ (‰)	-13.4	-13.3
$\epsilon_{app}^{15}N^a$ (‰)	-23.0	-22.4
$\epsilon_{app}^{15}N^b$ (‰)	-9.4	-7.1

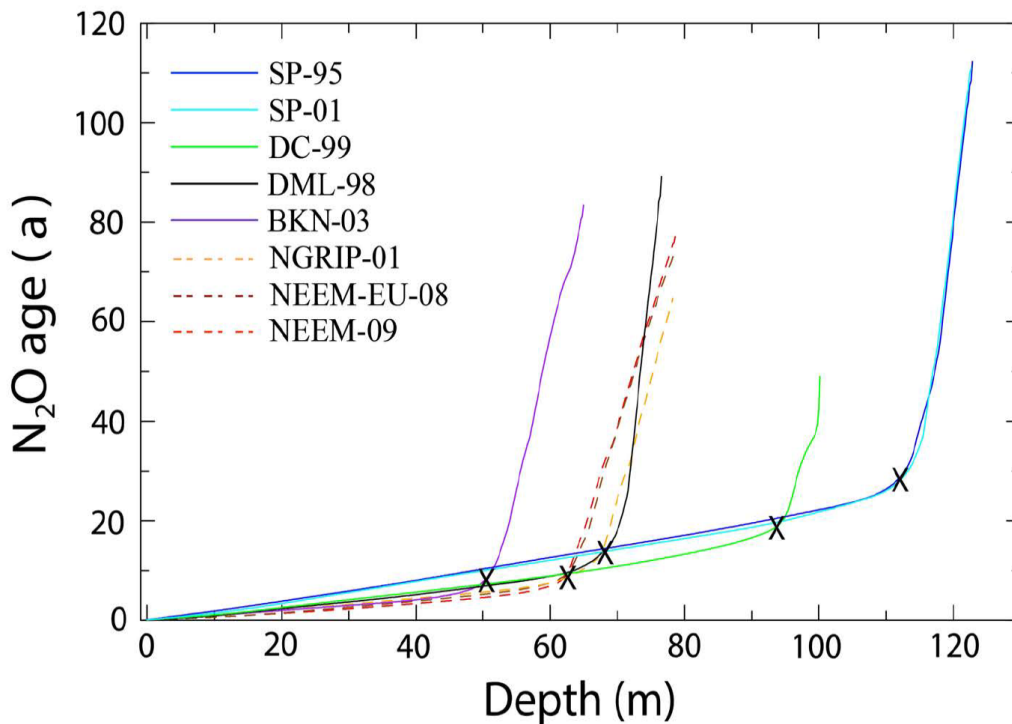
N₂O Lifetime (a)

This study**Park et al. (2012)**

123⁺²⁹₋₁₉120

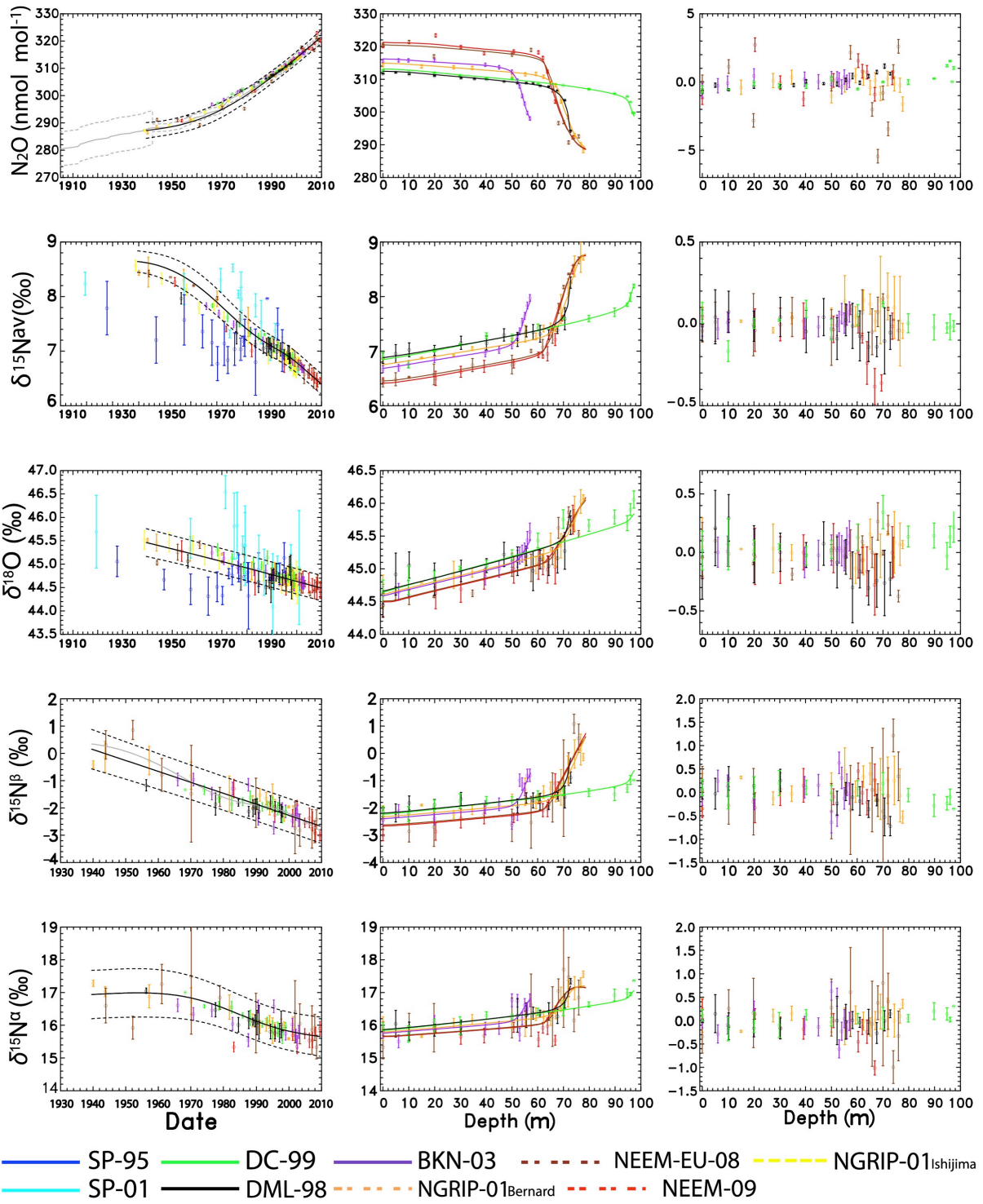
992 $^1\delta_{\text{atm,pi}}$ values are from Park et al. (2012) who also calculated $\delta_{\text{nat,pi}}$ and δ_{anth} in a two-box model. The values are (9.3 ± 0.2) (
993 ‰) for $\delta^{15}\text{N}^{\text{av}}$, (45.5 ± 0.2) (‰) for $\delta^{18}\text{O}$, (18.8 ± 1.0) (‰) and (-0.6 ± 1.1) (‰) for $\delta^{15}\text{N}^{\text{a}}$ and $\delta^{15}\text{N}^{\text{b}}$ respectively. In this study,
994 the δ_{anth} values are the averaged values over the whole investigated period. ϵ_{L} values used in this study are averaged values
995 from the lower stratosphere from Kaiser et al. (2006) and ϵ_{L} values from Park et al. (2012) were used from Park et al. (2004).

996



997

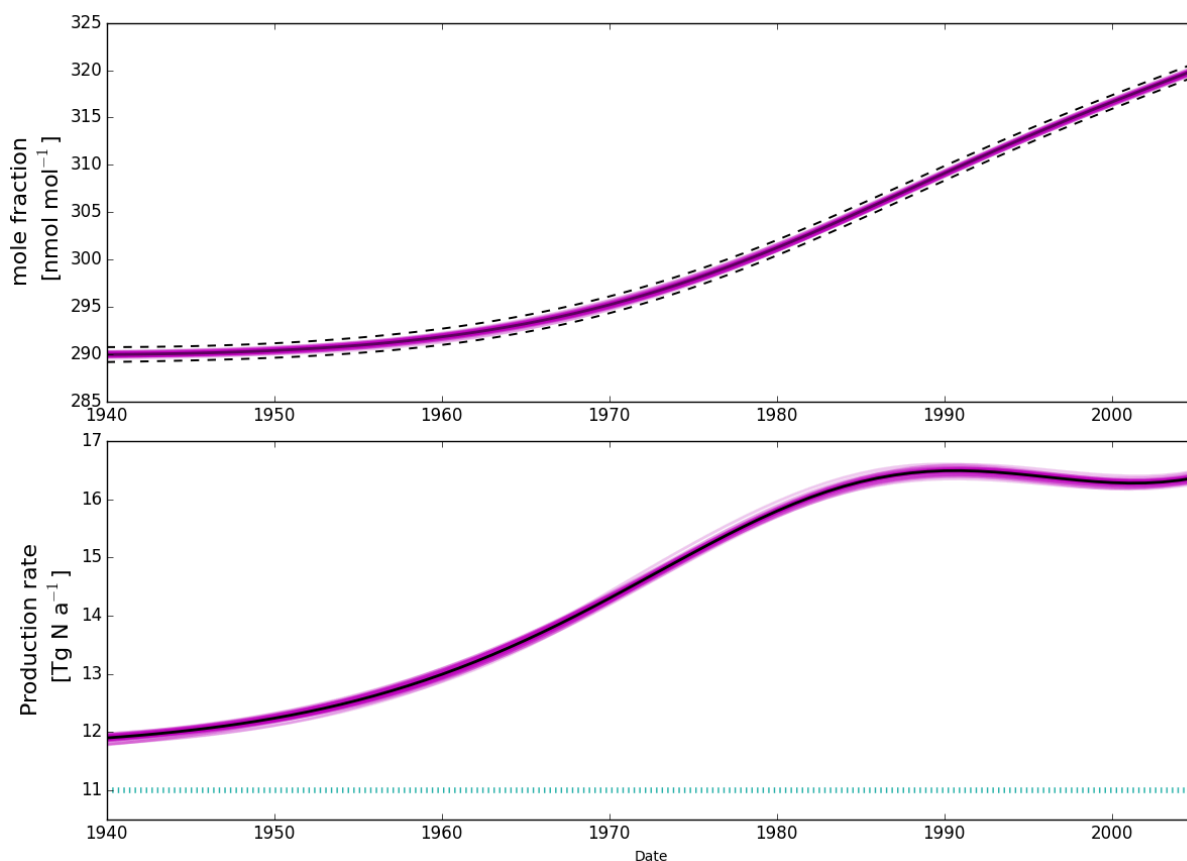
998 Figure 1. N₂O mean ages in firn versus depth. The dashed lines represent the sites from the
999 NH (North Greenland Ice-core Project [NGRIP-01 Bernard], North Eemian Ice-core Project
1000 [NEEM-09, NEEM-EU-08]) and the solid lines the SH sites (South Pole [SP-01, SP-95],
1001 Dome C [DC-99], Dronning Maud Land [DML-98] and Berkner Island [BKN-03]). The
1002 numbers accompanying the sites are the corresponding drilling years. Marker X indicates the
1003 transition between the firn diffusive zone and the bubble close-off zone for each site. Dashed
1004 orange line NGRIP-01, dashed brown NEEM-EU-08, dashed red NEEM-09, purple line
1005 BKN-03, black DML-98, green DC-99, blue SP-95 and light blue SP-01.



1006

1007

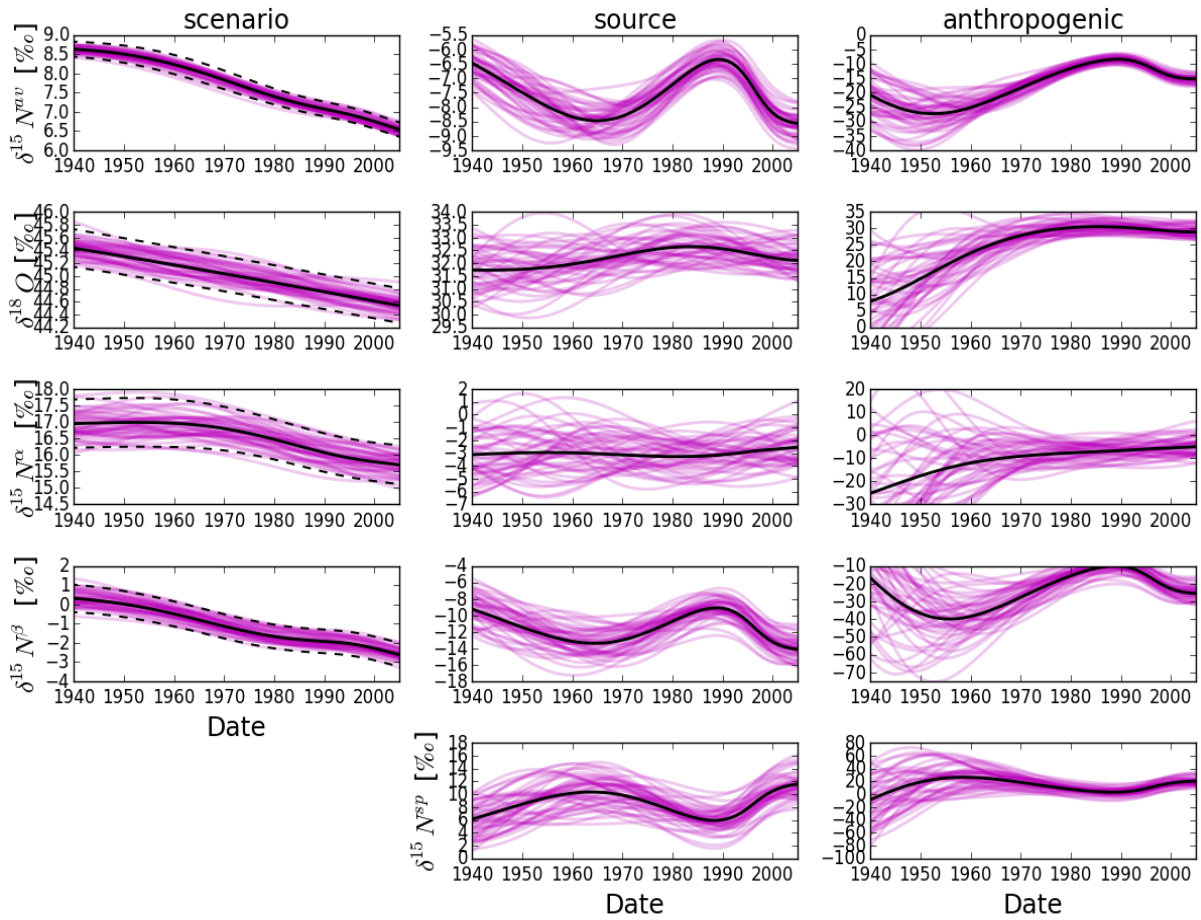
1008 Figure 2. Left: Reconstructed atmospheric scenarios (black solid line with dashed lines
 1009 indicating the 2σ uncertainty intervals) and results of the firm air samples (corrected for firm
 1010 fractionation) plotted at their respective assigned mean age. Middle: corresponding depth
 1011 profiles, symbols show the measurements and solid lines the results of the forward model
 1012 using the best estimate scenario as input. Right: model data discrepancies as a function of
 1013 depth. Orange: NGRIP-01_{Bernard}, Yellow: NGRIP-01_{Ishijima}, Brown: NEEM-EU-08, Red
 1014 NEEM-09, Purple: BKN-03, Black: DML-98, Green: DC-99, Blue: SP-95 and Light Blue:
 1015 SP-01. Data from NGRIP-01_{Ishijima} SP-95 and SP-01 were not used in the atmospheric
 1016 reconstruction and are only plotted for comparison purposes here.



1017
 1018 Figure 3: Top panel. N₂O mole fraction history constrained with the most precise data at
 1019 NEEM only to narrow the uncertainties (solid black line with uncertainty envelopes as dashed
 1020 black lines) and the scenarios within the uncertainty envelopes that were used in the mass
 1021 balance model (magenta lines) to evaluate the uncertainties of the atmospheric modelling
 1022 results.

1023 Bottom panel. N₂O production rate as calculated from the mass balance model. The solid
 1024 black line represents the result for the best fit reconstruction while magenta lines represent the

1025 results for the individual scenarios from the top panel. Dotted light green line denotes the
 1026 natural source emissions which were kept constant in our model runs.



1027

1028

1029 Figure 4: Left panels: Historic evolution of $\delta^{15}\text{N}^{\text{av}}$, $\delta^{18}\text{O}$, $\delta^{15}\text{N}^{\alpha}$ and $\delta^{15}\text{N}^{\beta}$ in N_2O as derived
 1030 from the firm air reconstruction. Middle panels: isotope signatures of the total emitted N_2O .
 1031 Right panels: isotope signatures of the anthropogenic source, respectively. The solid black
 1032 line represents the best-fit scenario while the dashed ones represent the respective
 1033 uncertainties as determined by the reconstruction method. Magenta lines represent the
 1034 emissions that are required to produce the magenta N_2O histories in the left panels.

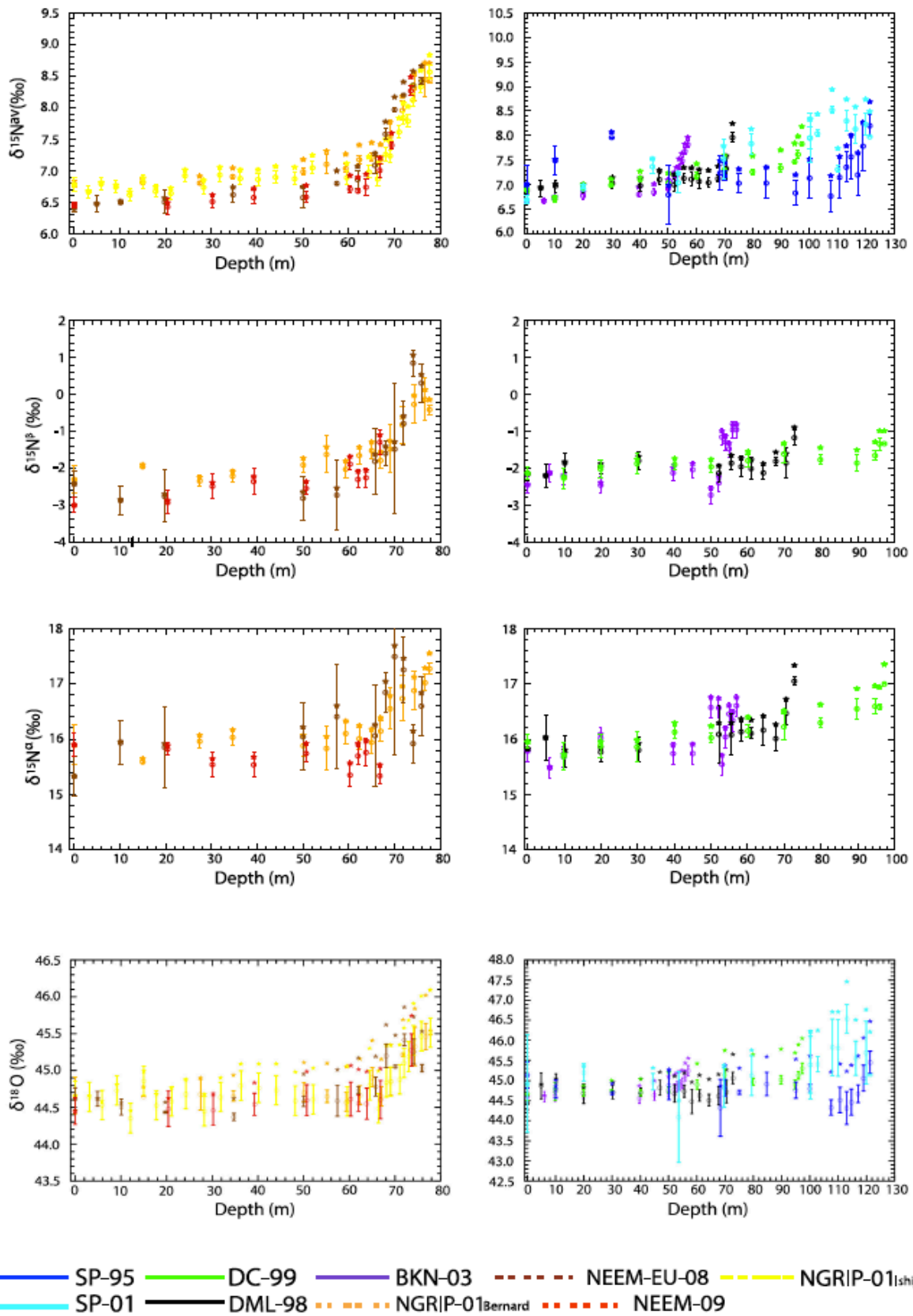
1035

1036

1037

1038

1039



1042 Figure A1: Effect of firn fractionation on N₂O isotopic composition in firn. Original
 1043 measurements are plotted as stars, data corrected for firn fractionation are plotted as circles
 1044 with error bars. The left hand side shows Northern hemisphere sites, orange: NGRIP-01_{Bernard},
 1045 yellow: NGRIP-01_{Ishijima}, brown: NEEM-EU-08, red NEEM-09 and the right hand side shows
 1046 Southern hemisphere sites, purple: BKN-03, black DML-98, green DC-99, blue SP-95 and
 1047 light blue SP-01

1048 **Appendix B: Data processing**

1049 In this study isotope deltas (δ) are used to denote the relative ¹⁵N/¹⁴N and ¹⁸O/¹⁶O ratio
 1050 difference of N₂O in firn air with respect to a standard reference,

$$1051 \delta^{15}\text{N} = \frac{R_{\text{sample}}}{R_{\text{standard}}} - 1 \quad (1)$$

1052 where R represents the ¹⁵N/¹⁴N or ¹⁸O/¹⁶O abundance ratio of a standard or a sample. $\delta^{15}\text{N}$
 1053 values are reported relative to ¹⁵R of atmospheric N₂, $\delta^{18}\text{O}$ values relative to ¹⁸R of Vienna
 1054 Mean Standard Ocean Water (VSMOW). The ¹⁵N/¹⁴N, ¹⁸O/¹⁶O and position dependent
 1055 ¹⁵N/¹⁴N isotope ratios were derived from measurement of the *m/z* 45 / *m/z* 44, *m/z* 46 / *m/z* 44
 1056 and *m/z* 31 / *m/z* 30 ion current ratios according to Kaiser et al., (2008), assuming a constant
 1057 ¹⁷O excess of 0.9 ‰.

1058 There is a disagreement between reported trends of the position dependent $\delta^{15}\text{N}^{\text{av}}$ values
 1059 reported in the literature from firn air on the one hand and archived air samples on the other
 1060 hand (Park et al., 2012; Ishijima et al., 2007; Bernard et al., 2006; Röckmann and Levin,
 1061 2005; Röckmann et al., 2003; Sowers et al., 2002). In principle the temporal trend measured
 1062 directly on archived air samples should be fully consistent with top firn air samples of the
 1063 various data sets, which were collected over a decade or more, since the air in the diffusive
 1064 zone is not very old. However, this is not the case. Using the high-precision determination of
 1065 the temporal trend of the N₂O isotope signatures on archived air samples from Röckmann and
 1066 Levin (2005) as reported in section 2.4 we rescale the different firn profiles to match this
 1067 trend in the diffusive zone by interpolating the measurements from the diffusive zone of all
 1068 sites to DC-99 (δ_{INT}). By using the firn model – assigned mean age of each sample, The
 1069 maximum age difference from diffusive zone to surface corresponds to $\Delta_{\text{age}} = \Delta_{\text{DC } t-t_0} = 10$ a.
 1070 Below you can find the equations used:

$$1071 \delta_{\text{INT}} = \delta_{t-t_0} - \delta_{\text{DC } t-t_0} + m (\Delta_{t-t_0} - \Delta_{\text{DC } t-t_0}) \quad (2)$$

1072 $\delta_{\text{Final}} = \delta_{\text{meas}} - (\delta_{\text{exp}} - \delta_{\text{INT}})$ (3)

1073 Where m is the slope connecting the two points we want to interpolate. The applied scaling
1074 (δ_{Final}) is given in the Table B1 below. To bring the data to the most recent international scale,
1075 NOAA-2006A, we used an equation extracted from a correlation between a scale ratio of
1076 NOAA-2006A to CSIRO versus the mole fraction of N₂O. The correlation showed higher
1077 scale ratio for low fraction values and lower scale ratio for higher mole fraction values. The
1078 equation extracted is given below:

1079 $y(\text{NOAA-2006}) = -1.535 \times 10^{-4} y^2(\text{CSIRO}) + 1.045 y(\text{CSIRO})$ (4)

1080 Table B1. Implemented scaling for N₂O mole fraction and isotopic composition. The re-
 1081 scaled average was extracted from the diffusivity zone for each site, which corresponds to the
 1082 top 50 m. The expected trends are averaged values from CSIRO
 1083 (<http://www.csiro.au/greenhouse-gases>) for the last 30 years for the mole fraction and
 1084 measured trends from Röckmann and Levin (2005) for the isotopic composition. The rather
 1085 large corrections to the isotope data from the SP-01 and SP-95 drillings are likely due to inter-
 1086 laboratory scale differences.

Site	$y(\text{N}_2\text{O})(\text{nmol mol}^{-1})$		
	Re-scaled average	Expected trend change	Correction
DML-98	0.09±0.29	-0.80±0.06	-0.89±0.32
NGRIP-01 _{Bernard}	3.39±0.54	1.60±0.06	-1.79±0.54
NGRIP-01 _{Ishijima}	4.12±0.32	1.60±0.06	-2.52±0.32
BKN-03	3.47±0.22	3.20±0.06	-0.27±0.23
NEEM-EU-08	3.57±1.81	7.20±0.06	3.63±1.81
NEEM-09	8.84±1.82	8.00±0.06	-0.84±1.82

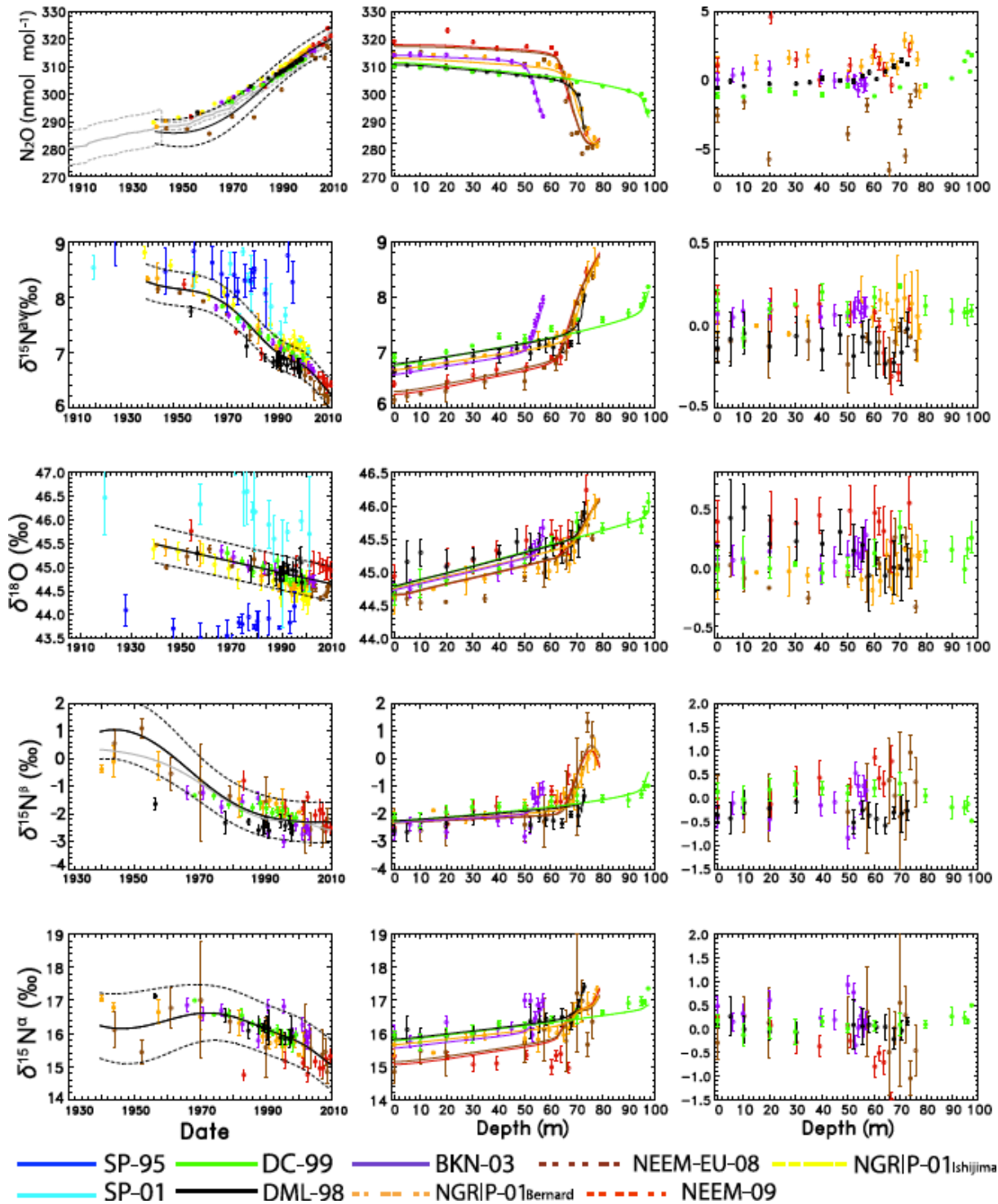
Site	$\delta^{15}\text{N}^{\text{av}} (\text{‰})$		
	Re-scale average	Expected trend change	Correction
SP-95	1.43±0.56	0.16±0.00	-1.27±0.56
DML-98	-0.18±0.12	0.04±0.00	0.22±0.12
SP-01	0.22±0.22	-0.08±0.00	-0.30±0.22
NGRIP -01 _{Bernard}	-0.18±0.07	-0.08±0.00	0.10±0.07
NGRIP -01 _{Ishijima}	0.17±0.13	-0.08±0.00	-0.25±0.13
BKN-03	-0.17±0.12	-0.16±0.00	0.01±0.12
NEEM-EU-08	-0.63±0.15	-0.36±0.00	0.27±0.15
NEEM-09	-0.43±0.05	-0.40±0.00	-0.03±0.05

Site	$\delta^{18}\text{O}$ (‰)		
	Re-scale average	Expected trend change	Correction
SP-95	-0.88±0.27	0.08±0.00	0.96±0.27
DML-98	0.26±0.15	0.02±0.00	-0.24±0.15
SP -01	0.74±0.62	-0.04±0.00	-0.78±0.62
NGRIP-01 _{Bernard}	-0.08±0.05	-0.04±0.00	0.04±0.05
NGRIP-01 _{Ishijima}	-0.17±0.12	-0.04±0.00	0.13±0.12
BKN-03	0.02±0.06	-0.08±0.00	-0.10±0.06
NEEM-EU-08	-0.21±0.15	-0.19±0.00	0.02±0.15
NEEM-09	0.28±0.04	-0.21±0.00	-0.49±0.04

Site	$\delta^{15}\text{N}^{\beta}$ (‰)		
	Re-scale average	Expected trend change	Correction
DML-98	-0.41±0.20	0.06±0.02	0.47±0.20
NGRIP-01 _{Bernard}	-0.10±0.25	-0.13±0.02	-0.02±0.25
BKN-03	-0.53±0.30	-0.26±0.02	0.27±0.30
NEEM-EU-08	-0.33±0.27	-0.58±0.02	-0.25±0.27
NEEM-09	-0.14±0.17	-0.64±0.02	-0.50±0.17

Site	$\delta^{15}\text{N}^{\alpha}$ (‰)		
	Re-scale average	Expected trend change	Correction
DML-98	0.09±0.11	0.01±0.02	-0.08±0.11
NGRIP-01 _{Bernard}	-0.26±0.19	-0.03±0.02	0.23±0.19
BKN-03	0.19±0.32	-0.06±0.02	-0.25±0.32
NEEM-EU-08	-0.61±0.35	-0.13±0.02	0.48±0.35
NEEM-09	-0.72±0.16	-0.14±0.02	0.58±0.16

1087 **Appendix C: Atmospheric reconstruction re-scaled to NEEM-09 and without**
 1088 **data re-scaling**



1089
 1090 Figure C1. Results of the firm data evaluation (similar to Figure 2) using the data without re-
 1091 scaling as indicated in the text, Orange: **NGRIP-01_Bernard**, Yellow: **NGRIP-01_Ishijima**, Brown:
 1092 NEEM-EU-08, Red: NEEM-09, Purple: BKN-03, Black: DML-98, Green: DC-99, Blue: SP-
 1093 95 and Light Blue: SP-01.

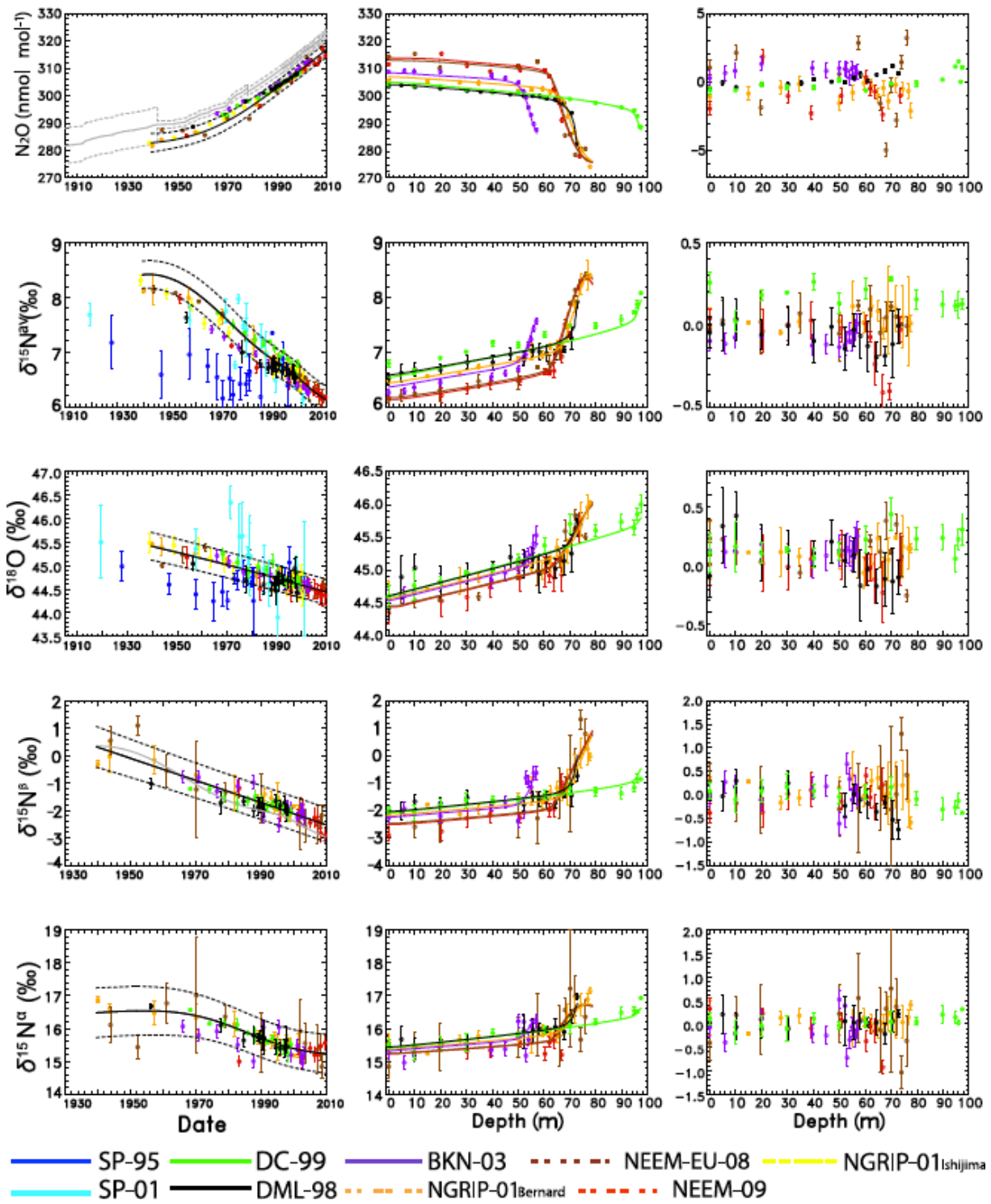
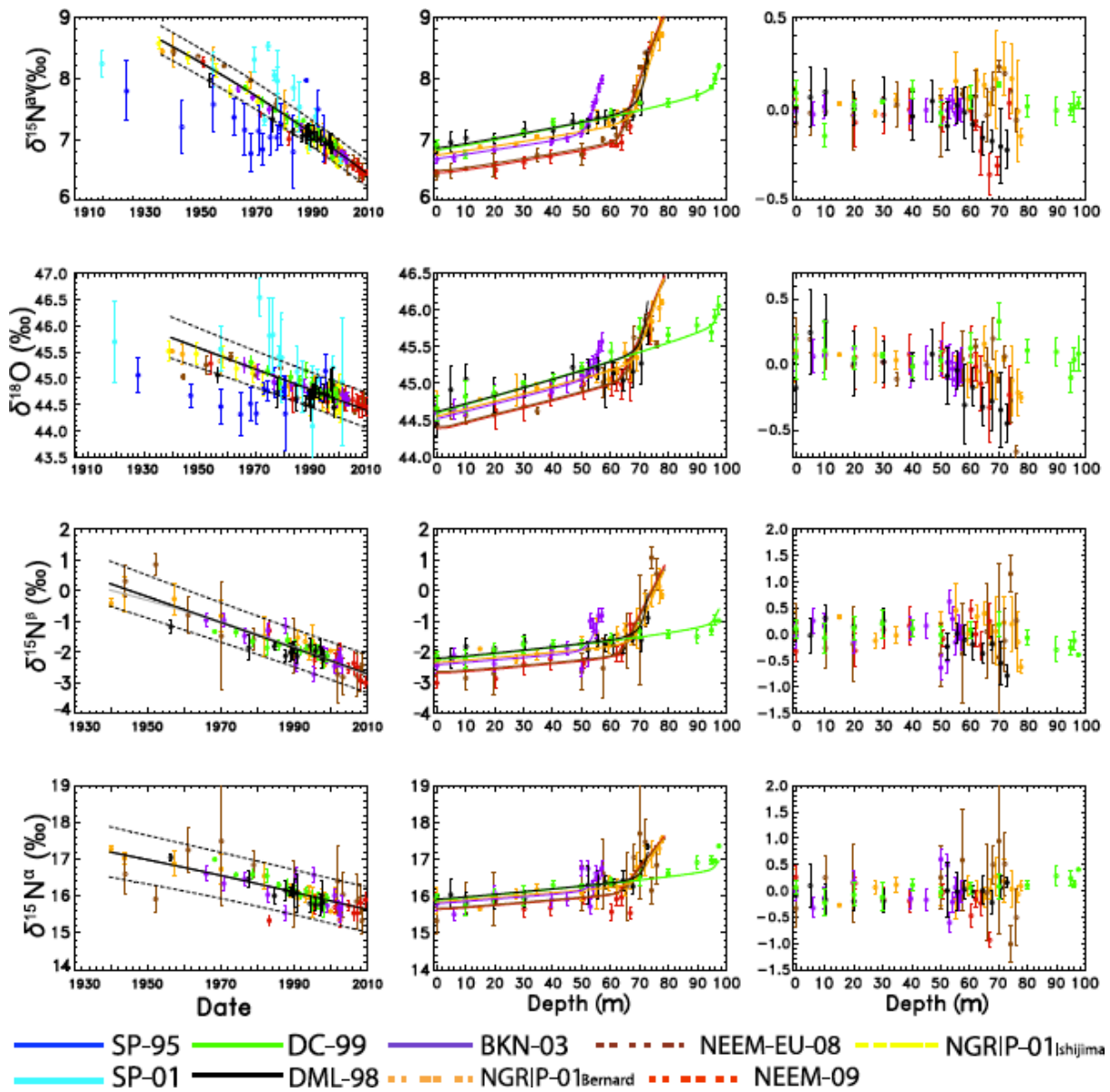
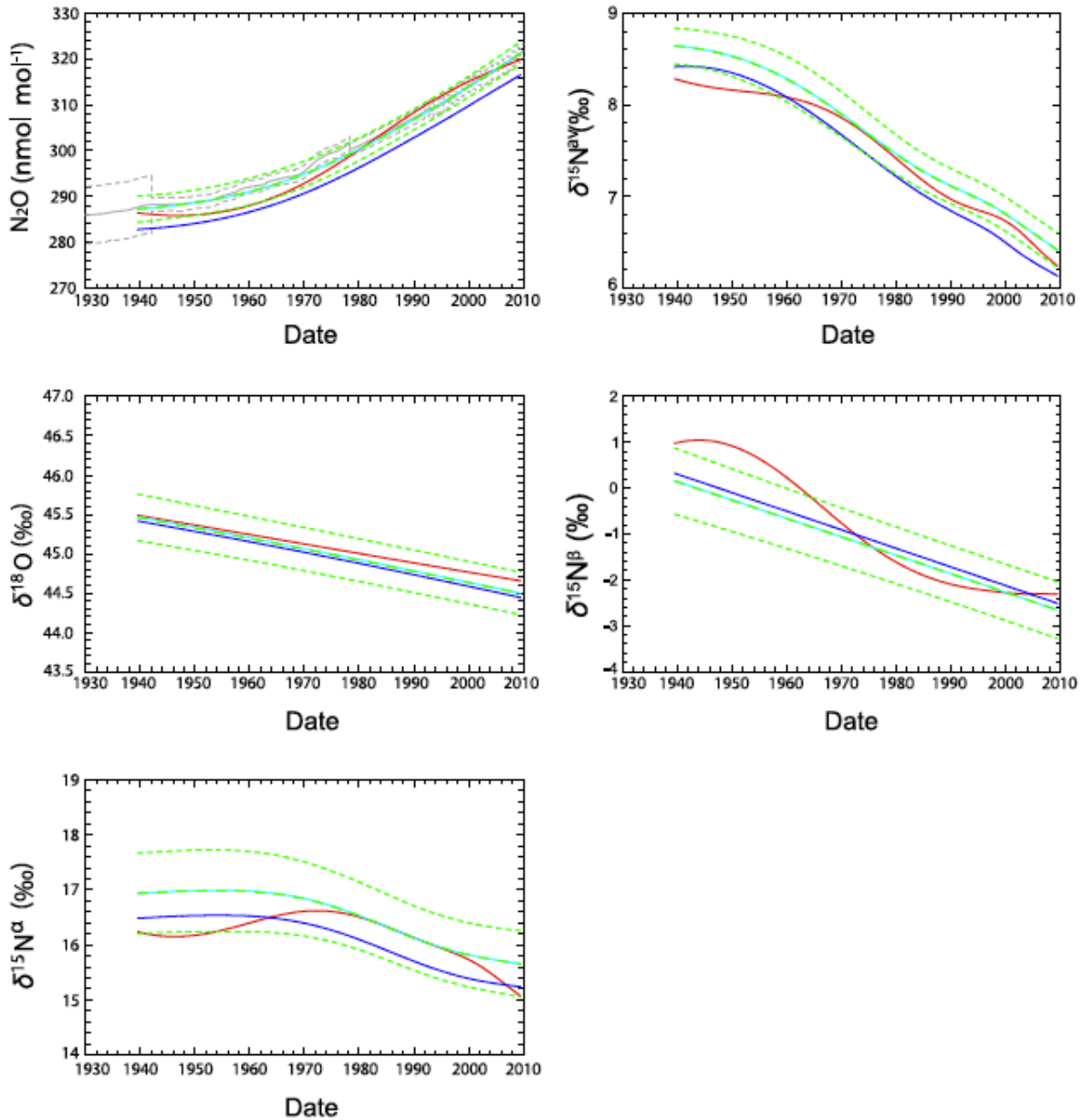


Figure C2. Results of the firn data evaluation (similar to Figure 2) using the data re-scaled to the NEEM-09 site. Colours as in Fig. C1.





1103

1104 Figure C4. Comparison of the atmospheric reconstructions between different re-scaling
 1105 methods. Solid and dashed green lines are the scenarios from data re-scaled to DC-99 used in
 1106 this study. Solid red lines are the best-case scenario for the non re-scaled data and solid blue
 1107 lines are the best-case scenarios from the data re-scaled to NEEM-09. The latter data series is
 1108 shifted because of a calibration offset. When this is corrected for the data superimposes the
 1109 green lines as expected.

1110

1111 **Appendix D: Sensitivity of the reconstructed N₂O emissions and isotopic**
1112 **signatures on N₂O lifetime.**

1113 For the default calculations with the mass balance model a constant lifetime for N₂O was
1114 used. A recent study from Prather et al. (2015), though, highlighted that top-down model
1115 calculations are sensitive to changes in the N₂O lifetime. To quantify the effect on our results
1116 we performed a sensitivity test where we linearly changed the N₂O lifetime from pre-
1117 industrial to modern times from 123 a in 1700 to 119 a in 2008. We also included runs with
1118 the absolute mean value changes in the assumed mean lifetime. The results are shown in
1119 Figures D1 and D2 below.

1120 In Figure D1 the N₂O atmospheric budget is re-calculated and compared with the results when
1121 the constant lifetime of 123⁺²⁹₋₁₉ a is used. In year 1940 the N₂O emissions are (12.3±2.7) Tg a⁻¹
1122 N and (17.0±1.7) Tg a⁻¹ N in year 2008 with a total increase of (4.7±1.7) Tg a⁻¹ N. When
1123 keeping the lifetime constant, the results for the same years are (11.9±1.7) Tg a⁻¹ N and
1124 (16.4±1.7) Tg a⁻¹ N with a total increase of (4.5±1.7) Tg a⁻¹ N. In addition, when looking also
1125 into the absolute mean value changes in the assumed mean lifetime we only observe a vertical
1126 shift of the scenarios that do not affect the temporal change. This shows that there is a
1127 sensitivity on the choice of lifetime for our mass balance model on the N₂O atmospheric
1128 budget as was indicated by Prather et al. (2015).

1129 The N₂O source isotopic signature shows no significant change with the choice of lifetime
1130 giving similar average source values for all source signatures as for when using a constant
1131 lifetime of 123⁺²⁹₋₁₉ a.

1132 On the other hand, the N₂O average anthropogenic source signature displays a sensitivity in
1133 the choice of lifetime returning values (-15.9±2.6) ‰, (28.5±2.6) ‰, (-7.2±1.7) ‰ and (-
1134 22.8±8.4) ‰ for $\delta^{15}\text{N}^{\text{av}}$, $\delta^{18}\text{O}$, $\delta^{15}\text{N}^{\alpha}$ and $\delta^{15}\text{N}^{\beta}$ respectively. This agrees within combined
1135 errors with the total average values of (-18.2±2.6) ‰, (27.2±2.6) ‰, (-8.1±1.7) ‰ and (-
1136 26.1±8.4) ‰ for $\delta^{15}\text{N}^{\text{av}}$, $\delta^{18}\text{O}$, $\delta^{15}\text{N}^{\alpha}$ and $\delta^{15}\text{N}^{\beta}$ respectively when a constant 123⁺²⁹₋₁₉ a lifetime
1137 is used. On average, the N₂O anthropogenic signature results can differ by 10 % when a
1138 different lifetime is chosen, which is equivalent to a (2.0±1.0) ‰ difference in the final
1139 anthropogenic values.

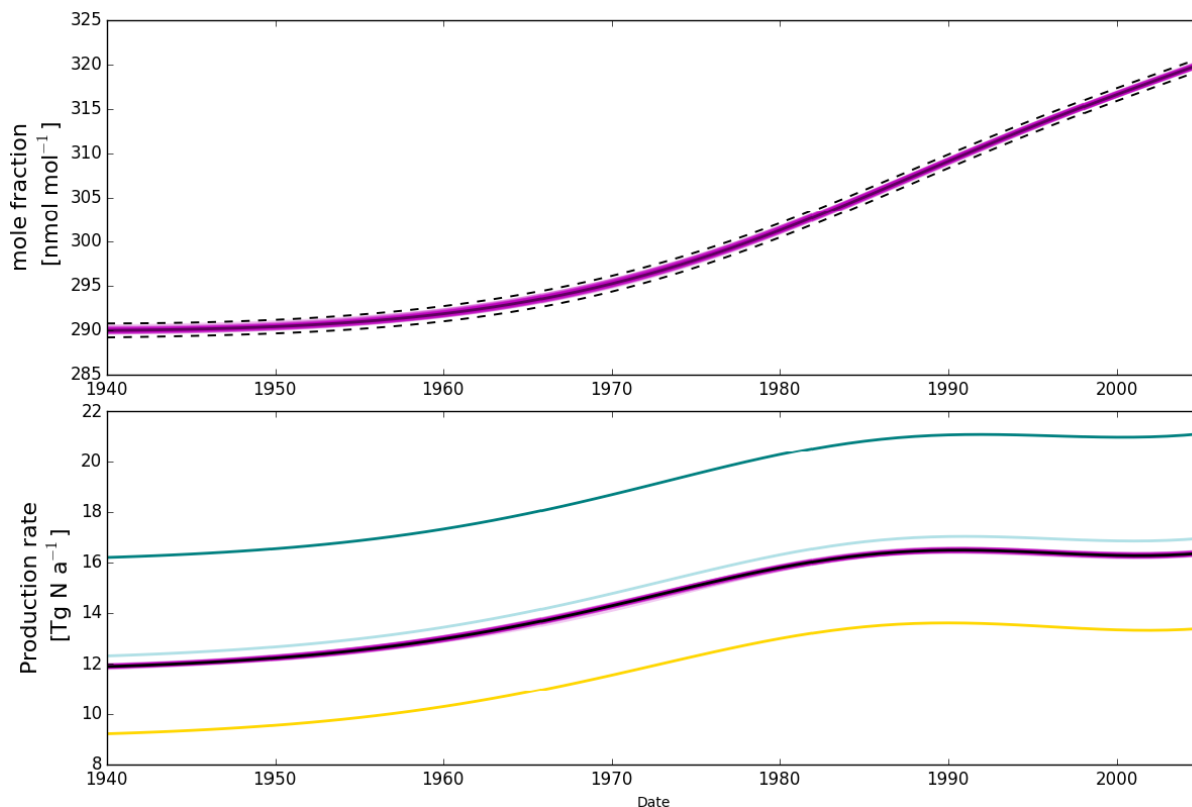
1140 Sensitivity tests were also performed on the F_{exch} parameter which gives us the annual fluxes
1141 between the two reservoirs (stratosphere - troposphere). Following Appenzeller et al. (1996)

1142 and Holton et al. (1990) the value was tested at a low and high value of 0.16 and 0.28 Tmol s⁻¹
1143 respectively with the one used in the manuscript being 0.22 Tmol s⁻¹. Results are shown in
1144 figures D3 and D4 below.

1145 In Figure D3 (middle panel) the atmospheric budget is re-calculated and compared to the
1146 optimal scenario values. At the bottom panel the air returned to troposphere from stratosphere
1147 is presented (F_{exch}). It is clear that when a low F_{exch} value is chosen, then less N₂O is returned
1148 to the troposphere. Contrary when a higher F_{exch} value is used more N₂O is returned.

1149 F_{exch} choice has little effect on the isotopic signature results as shown in Figure D4 and is
1150 mainly limited to the earliest part of the record (>1970) where the reconstruction uncertainties
1151 are larger. While it is expected when F_{exch} value is low the isotopic results to be more
1152 enriched compared to higher F_{exch} , in our case this is not clear from the test. The overall
1153 averaged values have a less than 2 % difference compared to the chosen (optimal) scenario
1154 and results of total averaged source and anthropogenic isotopic signatures are well within
1155 agreement with combined uncertainty errors in both total source and anthropogenic signatures
1156 respectively.

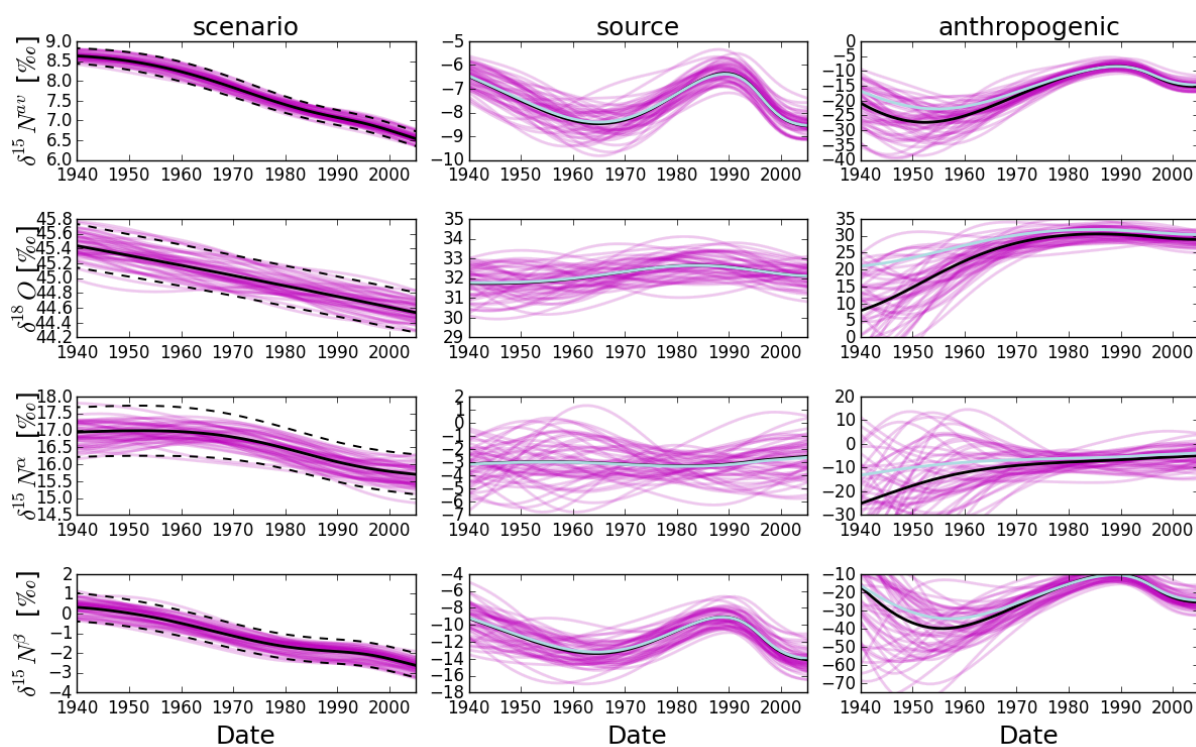
1157 Thus, we conclude that while the flux is indeed sensitive on the F_{exch} choice value the isotopic
1158 composition is not.



1159

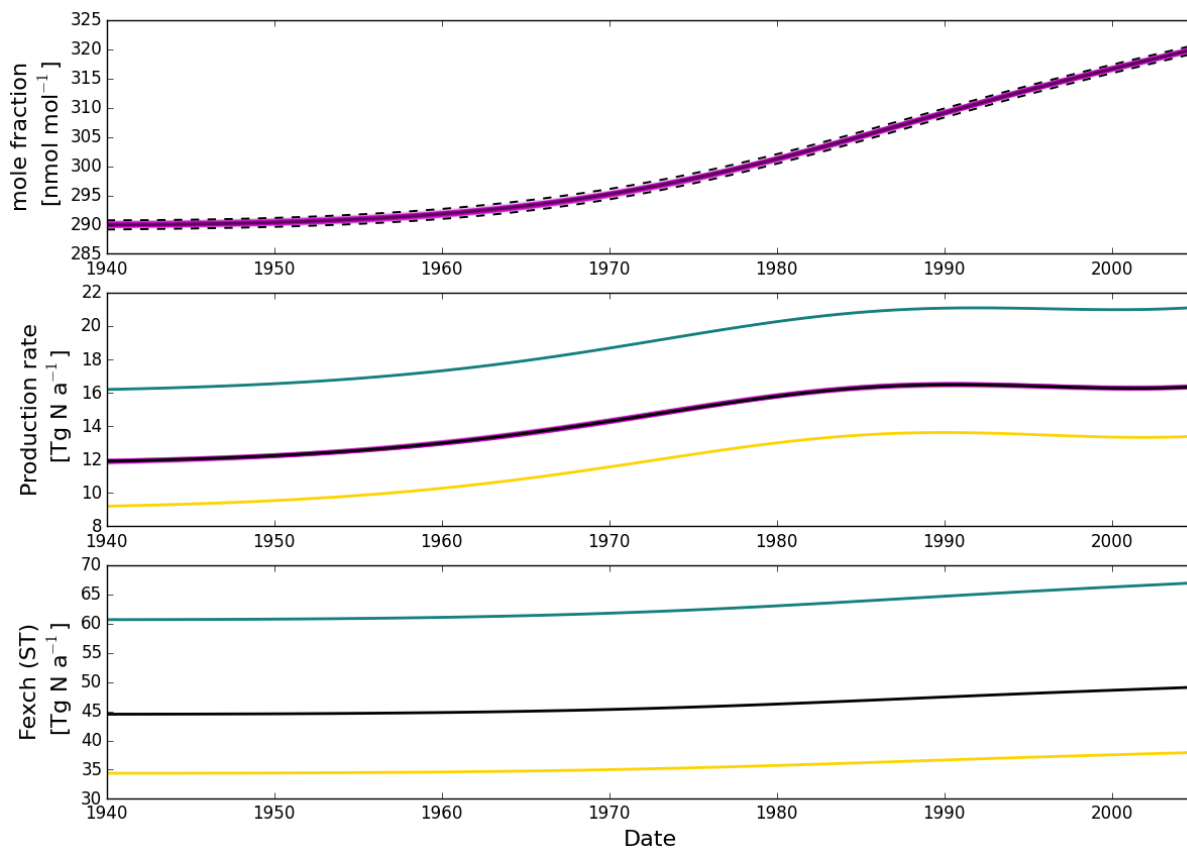
1160 Figure D1: Top panel. N₂O mole fraction history constrained with the most precise data at
 1161 NEEM only to narrow the uncertainties (solid black line with uncertainty envelopes as dashed
 1162 black lines) and the scenarios within the uncertainty envelopes that were used in the mass
 1163 balance model (magenta lines) to evaluate the uncertainties of the atmospheric modelling
 1164 results.

1165 Bottom panel. N₂O production rate as calculated from the mass balance model assuming a
 1166 change in the lifetime from 123 a in 1700 to 119 a in 2008 (relative change similar to Prather
 1167 et al., 2015) in light blue. The solid black line represents the result for the best fit
 1168 reconstruction while magenta lines represent the results for the individual scenarios from the
 1169 top panel (lifetime kept constant at 123⁺²⁹₋₁₉ a) as used in the main paper. Light green and
 1170 yellow show the results when lifetime is 154 a and 104 a respectively.



1171
 1172 Figure D2: Left panels: Historic evolution of $\delta^{15}\text{N}^{\text{av}}$, $\delta^{18}\text{O}$, $\delta^{15}\text{N}^{\alpha}$ and $\delta^{15}\text{N}^{\beta}$ in N₂O as derived
 1173 from the firn air reconstruction. The solid black line represents the best-fit scenario while the
 1174 dashed ones represent the respective uncertainties as determined by the reconstruction
 1175 method. Magenta lines represent the emissions that are required to produce the magenta N₂O
 1176 histories in the left panels. Middle and right panels: Isotope signatures of the total emitted

1177 N₂O and anthropogenic source respectively assuming a change in the lifetime from 123 a in
 1178 1700 to 119 a in 2008 (relative change similar to Prather et al., 2015) in light blue. The solid
 1179 black line represents the result for the best fit reconstruction while magenta lines represent the
 1180 results for the individual scenarios from the top panel (lifetime kept constant at 123_{-19}^{+29} a) as
 1181 used in the main paper.

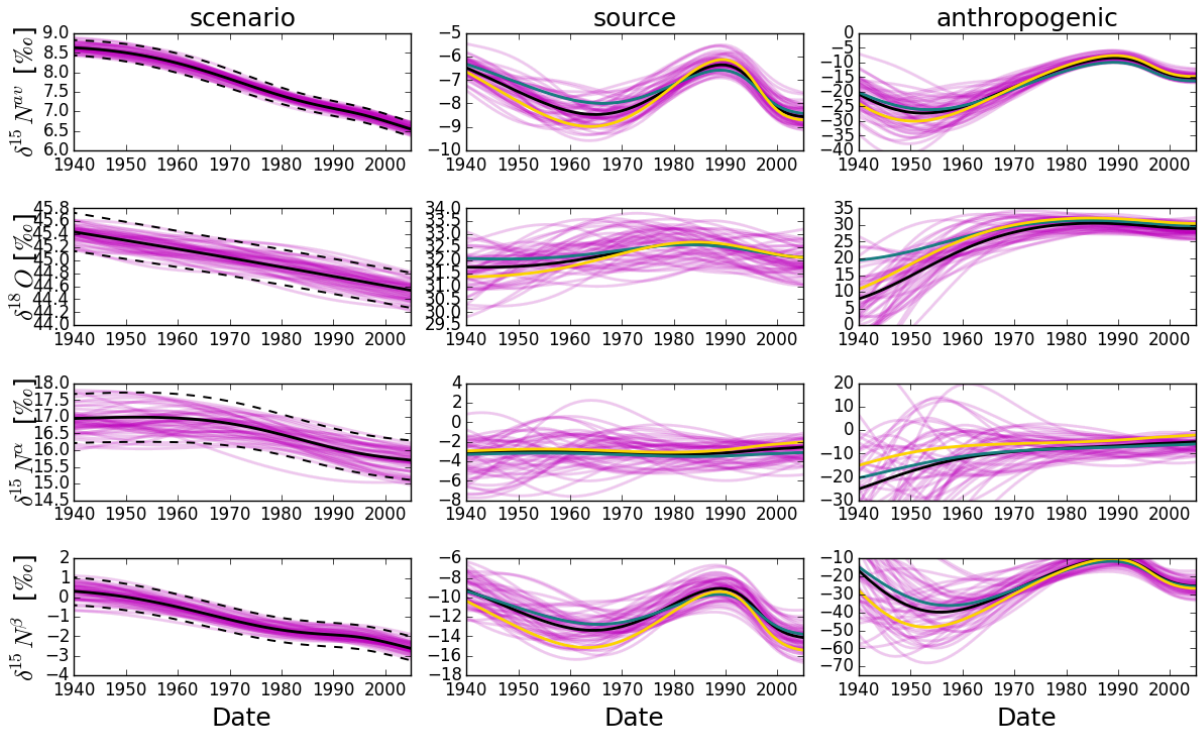


1182
 1183 Figure D3: Top panel. N₂O mole fraction history constrained with the most precise data at
 1184 NEEM only to narrow the uncertainties (solid black line with uncertainty envelopes as dashed
 1185 black lines) and the scenarios within the uncertainty envelopes that were used in the mass
 1186 balance model (magenta lines) to evaluate the uncertainties of the atmospheric modelling
 1187 results.

1188 Middle panel. N₂O production rate as calculated from the mass balance model assuming a
 1189 high (0.28 Tmol s^{-1}) F_{exch} in light green and a low (0.16 Tmol s^{-1}) value in yellow. The solid
 1190 black line represents the result for the best fit reconstruction while magenta lines represent the
 1191 results for the individual scenarios from the top panel as used in the main paper.

1192 Bottom panel. N₂O flux exchange results between stratosphere and troposphere as calculated
 1193 from the mass balance model assuming a high (0.28 Tmol s^{-1}) F_{exch} in light green and a low

1194 (0.16 Tmol s⁻¹) value in yellow. The solid black line represents the result for the best fit
 1195 reconstruction as used in the main paper.



1196
 1197 Figure D2: Left panels: Historic evolution of $\delta^{15}\text{N}^{\text{av}}$, $\delta^{18}\text{O}$, $\delta^{15}\text{N}^{\alpha}$ and $\delta^{15}\text{N}^{\beta}$ in N_2O as derived
 1198 from the firm air reconstruction. The solid black line represents the best-fit scenario while the
 1199 dashed ones represent the respective uncertainties as determined by the reconstruction
 1200 method. Magenta lines represent the emissions that are required to produce the magenta N_2O
 1201 histories in the left panels. Middle and right panels: Isotope signatures of the total emitted
 1202 N_2O and anthropogenic source respectively assuming high (0.28 Tmol s⁻¹) F_{exch} in light green
 1203 and a low (0.16 Tmol s⁻¹) value in yellow. The solid black line represents the result for the
 1204 best fit reconstruction while magenta lines represent the results for the individual scenarios
 1205 from the top as used in the main paper.